Chapter 5
Impact Cratering and Post-impact Sedimentation

Henning Dypvik, Morten Smelror, Atle Mørk, Stephanie C. Werner, and Trond H. Torsvik

5.1 Introduction

The impact origin of the Mjølnir structure has been confirmed by detailed studies of lithologies from two shallow boreholes; one close to the crater center (7329/03-U-01) and one 30 km NE from the crater periphery (7430/10-U-01) (Fig. 1.7). The boreholes revealed brecciated sediments containing shocked quartz grains. In 7430/10-U-01 a prominent ejecta layer with strong iridium enrichment has been recovered (Dypvik et al. 1996; Dypvik and Ferrell 1998; Dypvik and Attrep 1999; Sandbakken 2002) (see Figs. 6.2 and 6.3). In this chapter the Mjølnir core (7329/03-U-01) will be presented, whereas core 7430/10-U-01 is presented in Chap. 6.

Recent studies of marine impact targets and systematic compilations of their structural and morphological features have shown significant differences among impact craters formed on land and those formed at sea (Gersonde and Deutsch 2000; Ormö and Lindström 2000; Dypvik and Jansa 2003; Dypvik et al. 2004a; Gohn et al. 2008). The primary cause for several of these differences is the high water content in the sediments themselves, as well as the overlying sea water. These characteristics explain the rheological differences, and trigger different erosional and depositional processes that normally do not occur on land. During a marine impact, a water cavity is formed and modified by the growing crater rim and the ejecta curtain pushing the water outwards. Collapse of this water cavity starts at its base and causes a water flow towards the crater (Shuvalov 2002b). When the water depth is sufficient to overflow and cut through any uplifted rim, characteristic erosional/depositional resurge gullies can be formed, acting as inlets of water and material flowing back into the crater. This flow greatly affects the crater rim and leads to extensive infilling of the crater. In addition to the slumping, slides, avalanches and density currents are formed by the collapsing water-saturated sediments of the rim, the peak rings and

H. Dypvik (✉)
Department of Geosciences, University of Oslo, NO-0316 Oslo, Norway
e-mail: henning.dypvik@geo.uio.no

H. Dypvik et al. (eds.), *The Mjølnir Impact Event and its Consequences*, Impact Studies, DOI 10.1007/978-3-540-88260-2_5,

the central high. In the Mjølnir case, such complex sedimentation processes mixed sediments of variable lithologies from different stratigraphic levels of the pre-impact Upper Paleozoic and Mesozoic succession of the impact area. A detailed description of these rocks is given below.

5.2 The Mjølnir Crater Core (7329/03-U-01)

A shallow borehole (7329/03-U-01) was drilled into the Mjølnir crater at a water depth of 350 m in late August 1998 by the drillship M/S Bucentaur (Figs. 1.2, 1.6, and 1.7). A soil-drilling pipe was used to penetrate the 50-m-thick Quaternary sediment and till package (Fig. 5.1), and no samples were taken from this interval. An ordinary diamond drilling system placed inside the soil drilling pipe was used to core the bedrock. After every three meters of drilling, the core was retrieved using a wire-line system, then carefully extracted from the core barrel and a preliminary description made. Sonic velocity measurements and spectral gamma radiation analyses on the core were run where possible.

The coring operation went smoothly. The first 7 m of the marly limestones of the Klippfisk Formation were sampled, followed by 17 m of the grey, laminated shales of the Hekkingen Formation (Table 5.1 and Fig. 5.2). The rocks retrieved between 74.05 m below seabed and the core base at 171 m differed from anything else obtained in the Barents Sea. The core, however, had very low internal strength and pieces could not be lifted out of the core barrel without falling apart. The sound velocity could, therefore, not be measured regularly and only very low values were obtained, except in the few well-cemented intervals. The lack of core-strength prevented measurements of natural gamma activity aboard, and a technical breakdown that terminated the drilling operation made logging of the hole by ordinary petrophysical wire-line tools impossible.

After the core had been transported to the laboratory, and allowed to dry slowly, about 62 m had sufficient strength to be slabbed, and these parts were mounted in alumina trays as display cuts (Figs. 5.3–5.12). A spectral gammalog was recorded 4 years after drilling, using laboratory analyses analyses directly on the core (Fig. 5.13). Macrofossils, mainly from the Hekkingen Formation, were carefully extracted, together with samples for palynological and micropaleontological analyses (Fig. 5.14).

5.2.1 The Ragnarok Formation

The disturbed rocks cored between 171 and 74.05 m in borehole 7329/03-U-01 forms a mapable unit recognized within the Mjølnir crater, the so-called Ragnarok Formation formally described by Dypvik et al. (2004b) (Fig. 1.4). The occurrences of this unit are diagrammatically displayed in Figs. 5.2, 5.5, 5.6, and 5.8. They

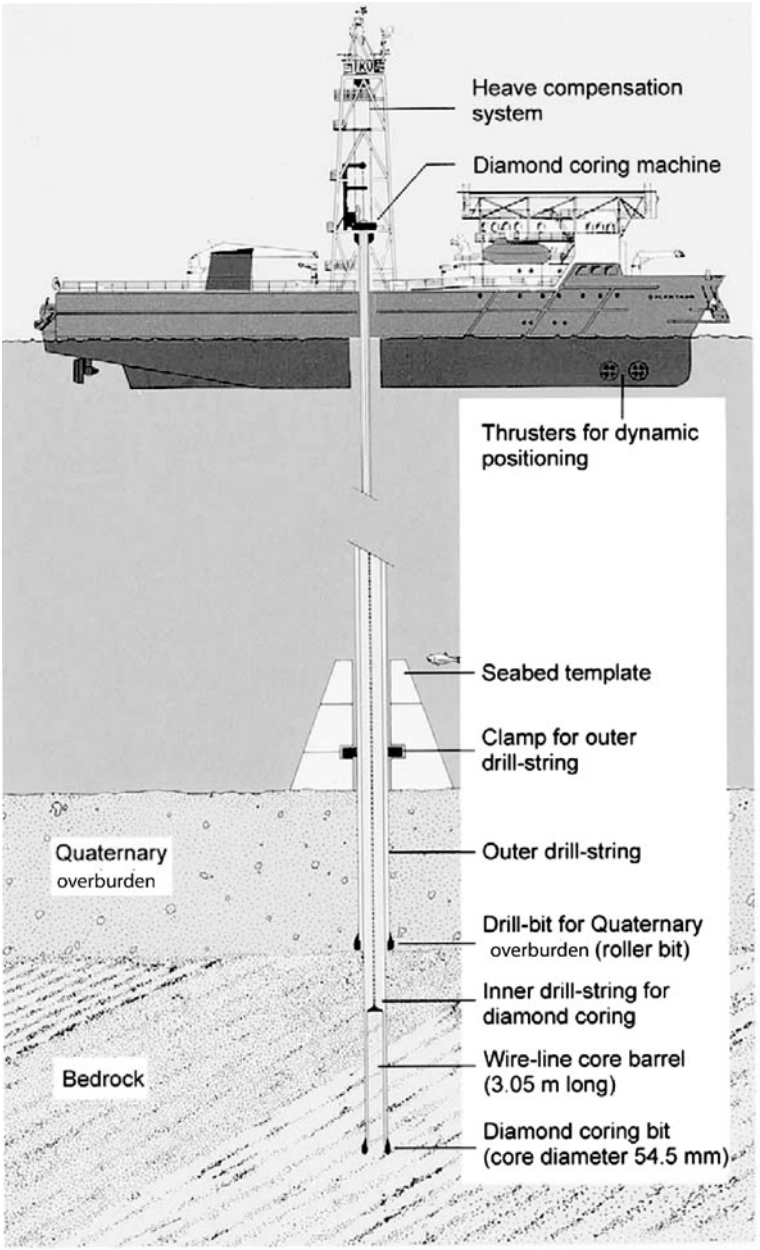

Fig. 5.1 The drilling device at Bucentaur RS, illustrating both overburden penetration and sediment coring

Table 5.1 A compilation of the stratigraphical subdivision, formation depths and lithological composition of the Mjølnir core (7329/03-U-01). Possible mechanism of deposition written in *italics*

Stratigraphic unit	Depth m	Lithology and interpration of depositional process
Klippfisk Fm	50.00–57.20	Very light greenish grey marls and carbonates, fossiliferous. Hemipelagic and pelagic rain
Hekkingen Fm	57.20–68.00	Light grey shales laminated, in some parts no fossils. From 63 m and up core rich in bioturbation. Hemipelagic rain
	68.00–73.78	Dark grey/black org.-rich shales, rich in fossils. Parallel lamination. Hemipelagic rain
	73.78–73.89	Interval with conglomerates and sandstones in mudstones. Storm-triggered turbidity currents
	73.89–74.05	Dark grey/black org.-rich shales, rich in fossils. Parallel lamination. Hemipelagic rain
Ragnarok Fm. subunit IIc	74.05–74.31	Matrix- and grain-supported, pebbly mudstone, faintly laminated. From level 74.05 to 75.73 mainly en-masse sediment transport possibly related to debris flow and/or turbidity current transport
	74.31–74.37	Parallel laminated, medium sandstones
	74.37–74.71	Massive, grain-supported conglomerate
	74.71–74.81	Medium sandstone, planar cross bedding, well sorted
	74.81–75.27	Clast- to matrix s.cgl., general inverse grading with faint cross bedding
	75.27–75.33	Fining-upwards sandstone with clay clasts, matrix supported
	75.33–75.42	Matrix-supported conglomerate, clay clasts
	75.42–75.48	Matrix-supported conglomerates with thin clay beds
	75.48–75.54	Mudstone with outsized clay clasts, matrix-supported
	75.54–75.61	Thin clay bed overlain by homogenous, clast-supported cgl
	75.61–75.73	Homogenous, clast-supported conglomerate
Ragnarok Fm. subunit IIb	75.73–79.50	Dark grey to brown, olive green, normally graded mudstone. Suspension fall-out
	79.50–83.00	Contains levels that are in situ brecciated (jig-saw
	83.00–87.43	puzzle fabric)
Ragnarok Fm. subunit IIa	87.43–87.70	Matrix supported conglomerate beds. Debris flow
	87.70–88.09	(mud flow)
	88.09–88.30	
	88.35–88.30	Siderite bed, septarian lower part and laminated darker brown upper part
Ragnarok Fm. unit I	88.35–171	Folded and fractured bedded sandstones, siltstones and shales with a few alternating carbonate beds. 120 cm monomict breccia at top of interval. Slumping and sliding of large sediment slabs

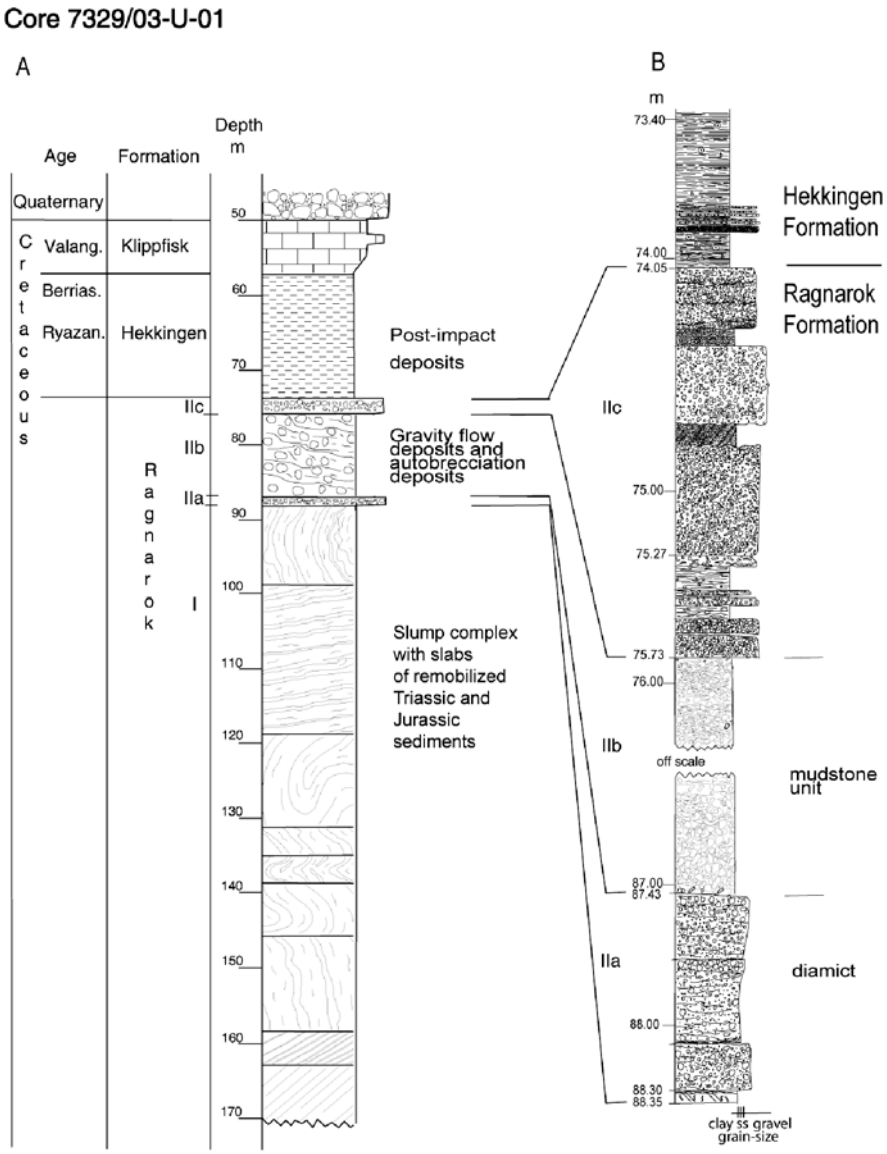

Fig. 5.2 The general core log of the Mjølnir core (7329/03-U-01) and detailed logs of the upper sedimentary formations. In the grain-size scale at the base of the sedimentary column, s s = silt and sand. Further details are presented in Figs. 5.5, 5.6, and 5.8, and in Chap. 8

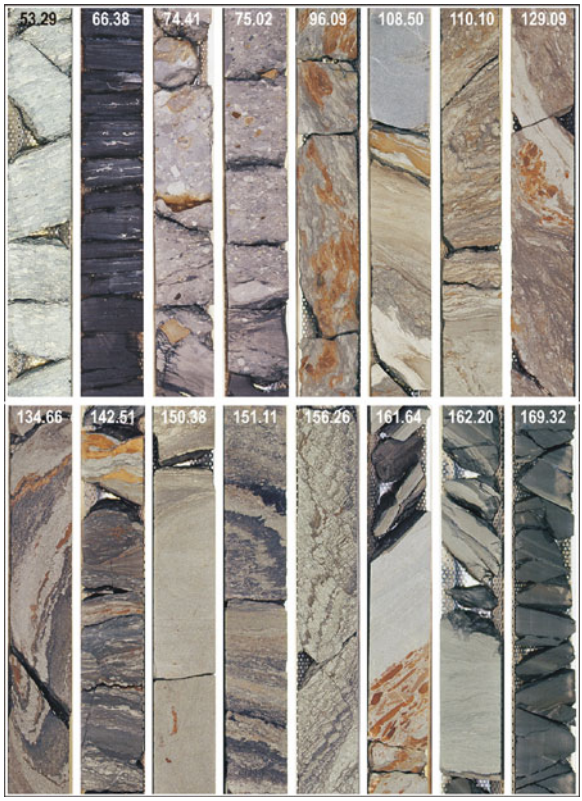

Fig. 5.3 Overview core photos of cut slices, the Mjølnir core (7329/03-U-01), depth level of top part is given at the cores. See the logs of Fig. 5.2 and Table 5.1 for stratigraphical positioning

consist of chaotic and avalanche- and slump-dominated sediments (unit I) (Figs. 5.3 and 5.4) overlain by avalanche and mass- and gravity-flow deposits (unit II) (Figs. 5.3–5.10). The units contain lithologies and rock fragments resembling rocks found in underlying stratigraphical units in the surrounding areas of the Barents Shelf and on Svalbard (Dypvik et al. 2004b, 2004c).

Core 7329/03-U-01 only penetrates the uppermost part (96.95 m) of the Ragnarok Formation (Table 5.1, Figs. 5.2 and 5.3). The base of the unit is presently defined according to seismic data. Its lower boundary is defined between the so-called autochthonous and allochthonous to parauthochtonous breccias, reaching 1.3 km depth below sea bed (Tsikalas et al. 1998a). This level represents a recognizable horizon on seismic data. The Ragnarok Formation consequently includes part of the structurally uplifted and slump-back deposits (parautochtonous breccias) (Figs. 5.3 and 5.4) and the fall-out/back and reworked/retransported resurge deposits (allochtonous breccias) (Figs. 5.3, 5.6, 5.9, and 5.10). The insitu and highly fragmented brecciated rocks formed during the excavation and modification stages in the transient crater, the so-called authochtonous breccias, are found below and were not reached by the core. The Ragnarok Formation is succeeded by the Hekkingen

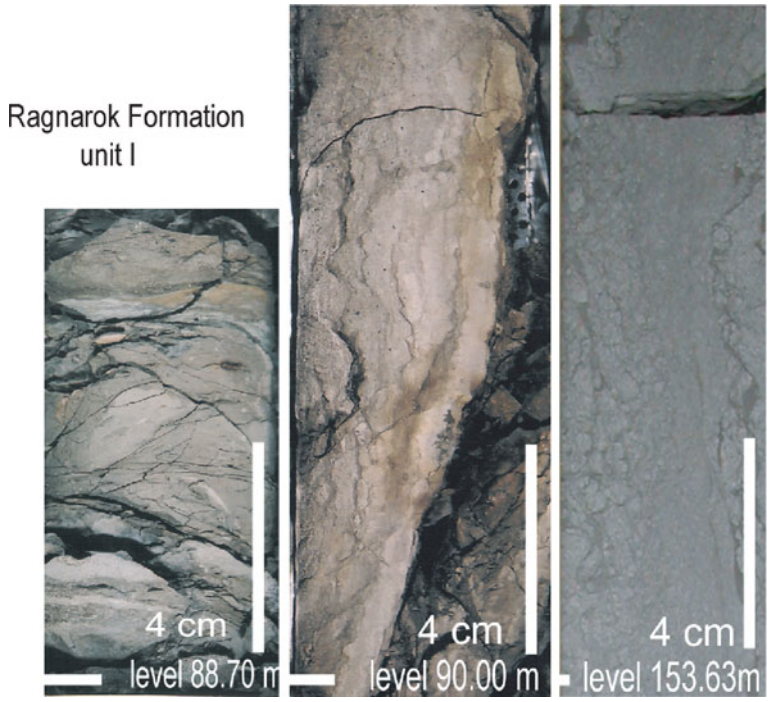

Fig. 5.4 Core photos of unit I, fractured and folded sedimentary successions. Details on their formation are presented in Chap. 8

and Klippfisk formations below a 50-m-thick Quaternary cover (Figs. 5.3, 5.11, and 5.12) (Mørk et al. 1999; Dypvik et al. 2004b, c).

Dating of the underlying and overlying sediments show the Ragnarok Formation was formed close to the Volgian-Ryazanian boundary time (Smelror et al. 2001a, b; Bremer et al. 2004; Smelror and Dypvik 2006). The formation, however, carries re-sedimented fragments, dominantly of late Early to Late Triassic ages, and to a lesser extent, of Jurassic age (see below).

Outside the Mjølnir crater rim, equivalents to the Ragnarok Formation are recognized on seismic data (Tsikalas et al. 2002a). As expected, the Hekkingen Formation is found above and below the Ragnarok Formation. The boundaries of this wedge in near crater areas have so far not been cored or sampled. The Sindre Bed, the ejecta unit and lateral equivalent of the Ragnarok Formation, represents the impact-related material outside the crater.

5.2.2 Ragnarok Formation, Unit I

Unit I (171–88.35 m) (Table 5.1, Figs. 5.2, 5.3, and 5.4) consists of strongly folded and fractured clay-, silt- and sandstones. These are described in detail and discussed

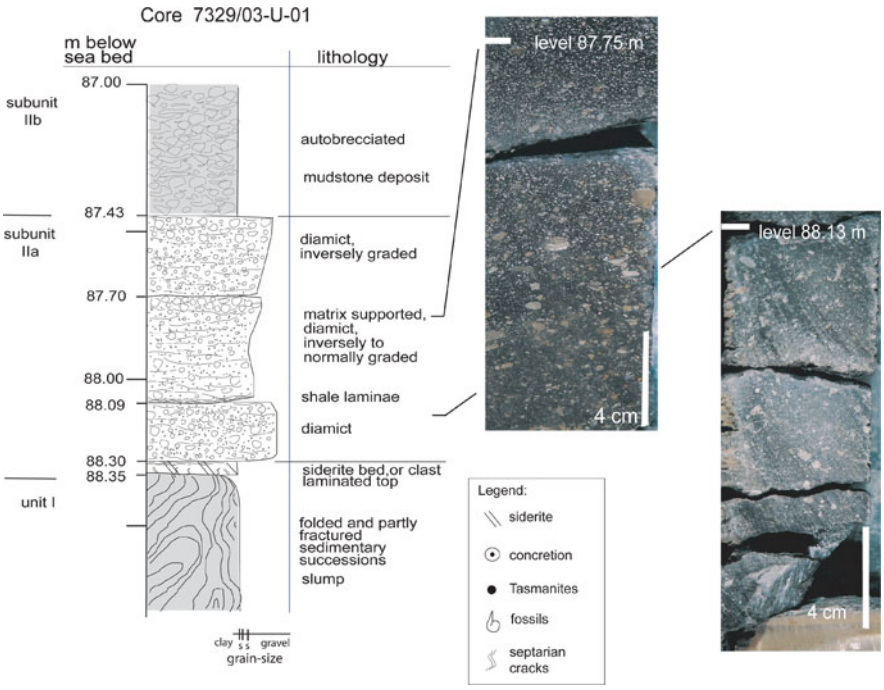

Fig. 5.5 Detailed core log of Unit IIa of core 7329/03-01. The matrix supported diamicts are illustrated as are the lower boundary to the siderite bed (88.13 m). In the grain-size scale at the base of the sedimentary column, s s = silt and sand

in Chap. 8. The palynomorph assemblages in this unit comprise a mixture of taxa derived from deposits of Spathian (late Early Triassic) to Late Jurassic age (see below, Fig. 5.14).

The degree of folding and faulting varies throughout the core and in some parts both vertical and horizontal bedding can be observed, often in combination with soft sedimentary deformation and water escape structures (see Chap. 8). Unit I is interpreted to represent reworked, folded and fractured pre-impact sediments, that were deposited as scree, avalanches, and slumps along the central peak of the crater (Dypvik et al. 2004a, b).

The uppermost 120 cm of unit I (Fig. 5.5) contains a fragmented, brecciated bed (89.55–88.35 m). The bed has a sharp upper boundary and an angular unconformity with an overlying siderite layer (Fig. 5.5) and the succeeding diamict of unit IIa. This 120 cm thick bed consists of partly folded clay clasts, grain-supported with a clayey matrix. The palynomorphs recorded from this unit are of the same ages as in the deposits below (Figs. 5.14 and 5.15). Lithologically, the clasts are similar to those just below this top part, dominated by grey claystones with a low content of silt and sand.

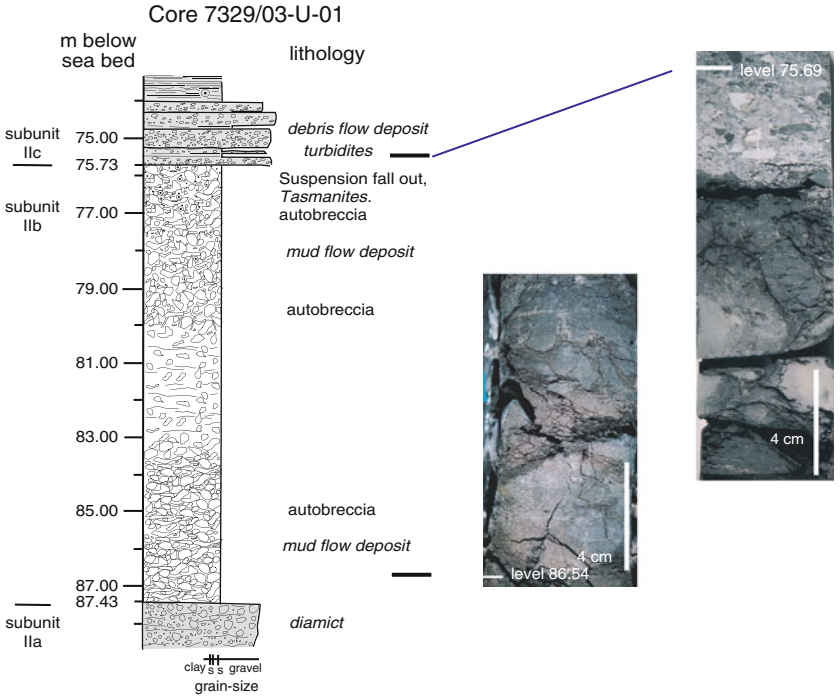

Fig. 5.6 Detailed core log of autobrecciated beds in Unit IIb of core 7329/03-01). In the autobrecciated part (between levels 75.73 and 87.43 m) the clasts and matrix have the same composition. In the grain-size scale at the base of the sedimentary column, s s = silt and sand

5.2.3 Ragnarok Formation, Unit II

Unit II (88.35–74.05 m) generally consists of poorly sorted conglomerates and can be divided into three subunits IIa, IIb and IIc (Figs. 5.2–5.10; Table 5.1).

Subunit IIa (88.35–87.43 m) consists of two well-defined parts: A lower, light brown, 5 cm thick, dense siderite bed or concretion (88.35–88.30 m), and an upper 87 cm thick (88.30–87.43 m) diamict with a dark grey, sandy clay matrix (Table 5.1 and Fig. 5.5). Septarian cracks are typically found in the lower 3.5 cm of the siderite bed. The upper 1.5 cm of the siderite shows a faint parallel lamination and is sharply separated from the overlying conglomerates but, shows similar orientation of bedding. The cored siderite may represent a siderite concretion, but the bedding being similar to the overlying sediments, indicates a possible in-situ origin associated with the diamicte above.

The major part (87 cm) of unit IIa is a homogeneous and poorly sorted diamict composed of a matrix-supported, dark grey, pebbly mudstone with subrounded to subangular clasts (Fig. 5.5). The intraclasts consist of sandy silt and claystone fragments up to about 2 cm in size, but with 2 mm as an average. The lithological

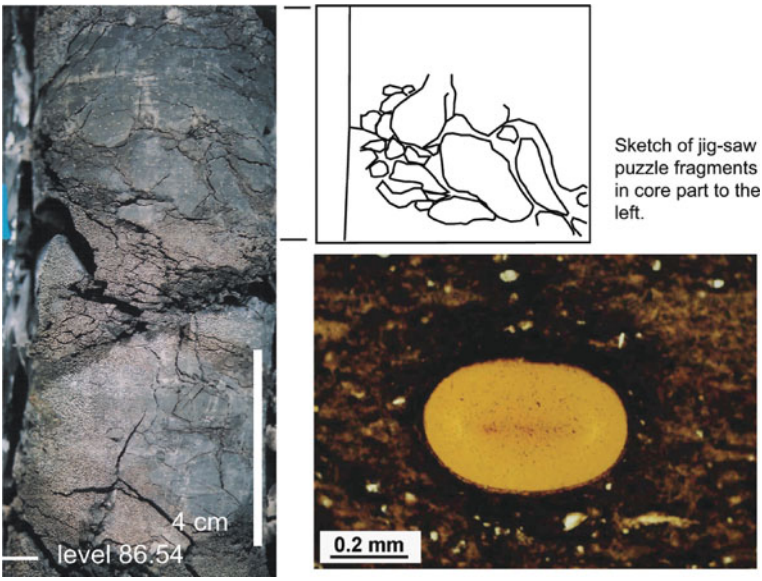

Fig. 5.7 Details of Unit IIb; *left core piece* with jigsaw puzzle clay clast, *upper right* a sketch of the fit of these clasts in the upper part of the core. The *lower right* shows a tasmanites fossils from Unit IIb

compositions of the clasts resemble the reworked Triassic and Jurassic sediments also found in unit I. Only faint clast-orientation has been observed in the pebbly mudstone (diamict). In Fig. 5.5 they seem to have their long axis parallel to horizontal, possibly indicating some shear movement. Glass/melt or glass/melt fragments have not been found so far. The sediments are poorly cemented and disintegrate easily in water, as does most of unit II.

The pebbly mudstones of unit IIa may be further subdivided into three minor parts that are separated by two cm-thick layers containing irregular shear laminae. The lowermost layer (88.30–88.10 m) is fairly homogeneous. The overlying section (88.10–87.70 m) shows faint layering and contains more lightly coloured, subrounded clasts especially in its upper part (87.85–87.70 m). This change in colour and roundness may reflect an additional input from a different source, but presently we do not have any good candidate. The uppermost section (87.68–87.43 m) shows some clast enrichments along its uppermost layers, but no changes in clast size (Fig. 5.5).

In the upper part of subunit IIa, the alga *Leiosphaeridia* is present in great abundance, as is also the case in the overlying Hekkingen Formation (Bremer et al. 2004). An algal bloom of *Leiosphaeridia* is also recorded in other correlative sediments and is attributed to increased nutrition of the seawater caused by the impact (Smelror et al. 2002). This indicates that the finest grained gravity deposited material of this subunit was deposited some time after the impact.

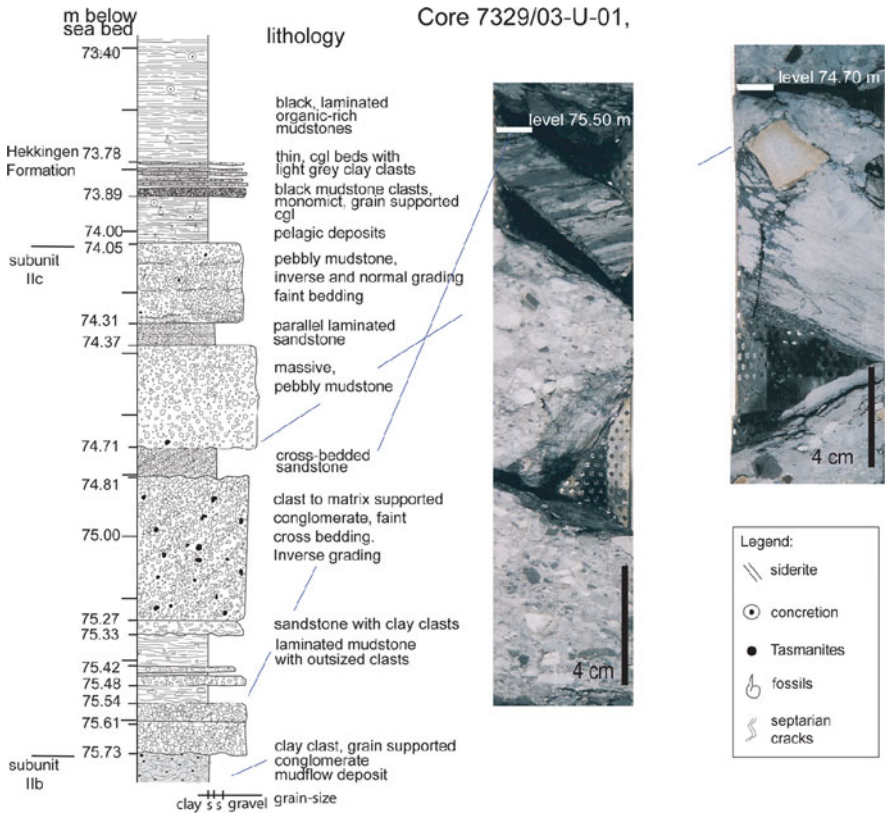

Fig. 5.8 Detailed core log of Unit IIc of core 7329/03-01. The unit consists mainly of conglomerates, sandstones and laminated mudstones. Detailed core photos in Fig. 5.9. In the grain-size scale at the base of the sedimentary column, s s = silt and sand

Subunit IIa most likely was deposited from debris or mud flows along the central peak, while the siderite bed may represent a diagenetic alteration product (Dypvik et al. 2004a, b). Unit IIa appears to represent the first collapse phase of the central peak, possibly tsunami related.

Subunit IIb (87.43–75.73 m) is an 11.70 m thick, homogenous unit consisting of dark grey to brown and olive green, highly fragmented claystones (Figs. 5.5, 5.6, and 5.7). Some few cm-sized siderite concretions are also present. The clast- and matrix-supported unit IIb displays clay clasts in a matrix of mud. The clay clasts are composed of similar material as the matrix and are difficult to distinguish macroscopically, but are easily distinguished in thin section with a more consolidated appearance than the matrix. The angular to subrounded clay clasts range in size from a few millimeters to 5 cm, indicating that the clay must have been somewhat compacted/consolidated before they were reworked.

The disintegrated clay clasts and matrix together consist of more than 90% coarse clay and fine silt, with average grain sizes between 3 and 13 μm (Dypvik et al.

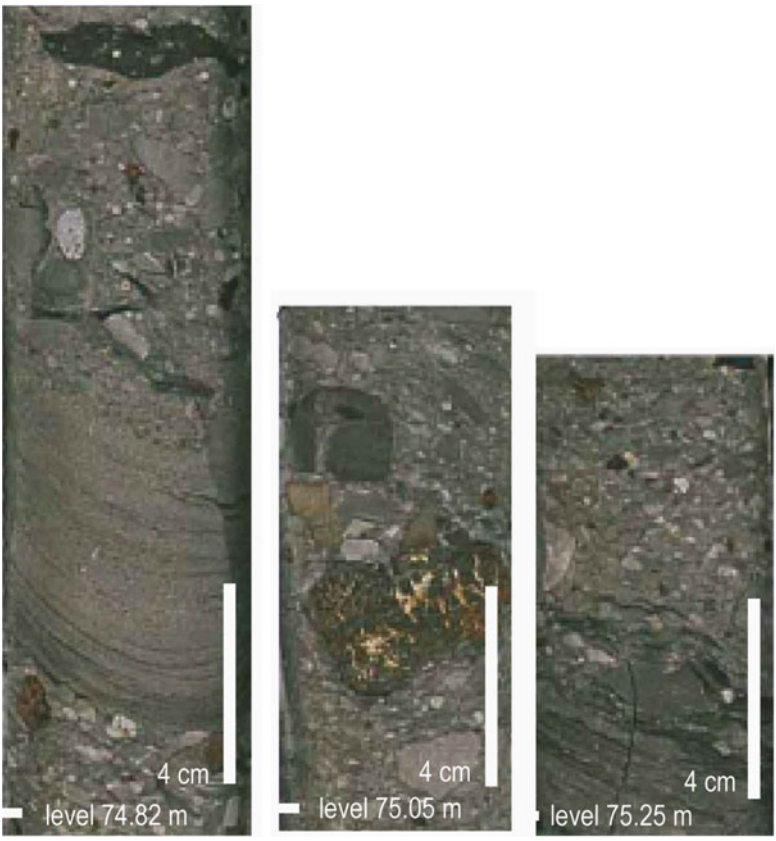

Fig. 5.9 Core photos Unit IIc; displaying conglomeratic and laminated sandstone sections. The location in core is shown in Fig. 5.8

2004b, c). In the uppermost parts of the unit indications of bimodal grain size distribution are seen, with minor enrichments at 40–50 μm grain size. The grain-size distribution in unit IIb can generally be characterized as unimodal, with a slightly fining upward trend. The subunit does not show any obvious bedding, except for a faintly laminated and apparently almost clast free interval between 83 and 81 m (Fig. 5.6). At few levels (incl. 79.4 m) chemical alteration structures are seen as somewhat lighter bands that cut the core. Brownish alteration bands and spots are found sporadically, and are most likely secondary diagenetic feature.

Recycled palynomorphs in the subunit are of mixed Early Triassic (Spathian) to Jurassic age (Fig. 5.14). In the uppermost 2.5 m of subunit IIb, the prasinophyte alga *Tasmanites* is found together with 1–3 cm large pyrite concretions. The recorded *Tasmanites* are around 0.5 mm black spheres. In thin sections, they have a well-defined orange (light) to green appearance under crossed polars (Fig. 5.7). *Tasmanites* algae of similar size are abundant in Middle Triassic sediments on

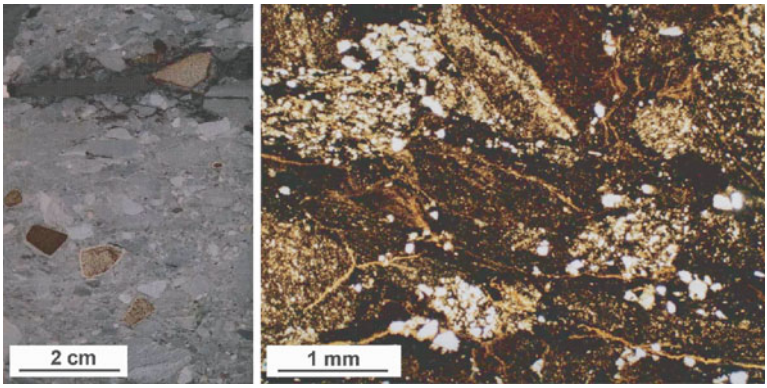

Fig. 5.10 Core photo (*left*) and thin section photo (*right*) of Unit IIc. The light oxidation rims on a couple of grains are well developed in the *left photo*

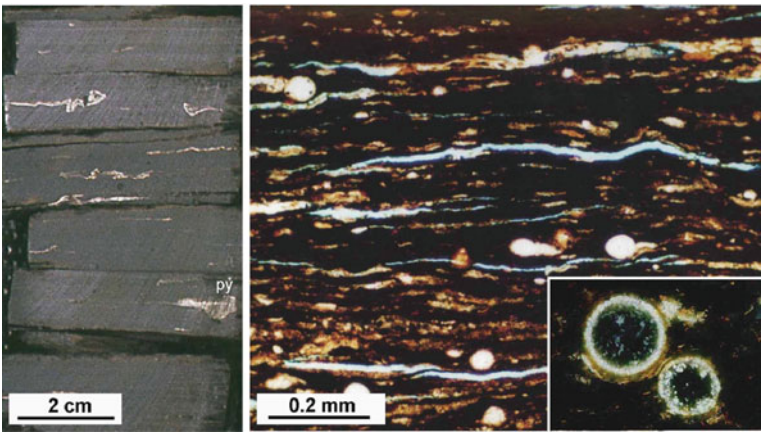

Fig. 5.11 Core photo (*left*) and thin section photos (*right*) of the Hekkingen Formation. In the *left photo* fine laminated black shales with light Buchias and pyrite concretion (py) is shown. In the *right photo* the thin section of this finely laminated shale show a large content of spheridal algae (*inset*)

Svalbard and in Northern Barents Sea cores (A. Mørk and J.O. Vigran, personal communication).

Subunit IIb most likely represents mud flow deposits formed by autobrecciation, possibly in relation with the tsunami reworking and the major modification phase of the crater (Dypvik et al. 2004b). The upper boundary towards subunit IIc is a sharp, well-defined erosional surface, which may have been caused by the succeeding density flows of subunit IIc (Figs. 5.6 and 5.8).

Subunit IIc (75.73–74.05 m) has a composition characterized by well-defined diamict, conglomerates and minor sandstone beds (Figs. 5.8, 5.9, and 5.10,

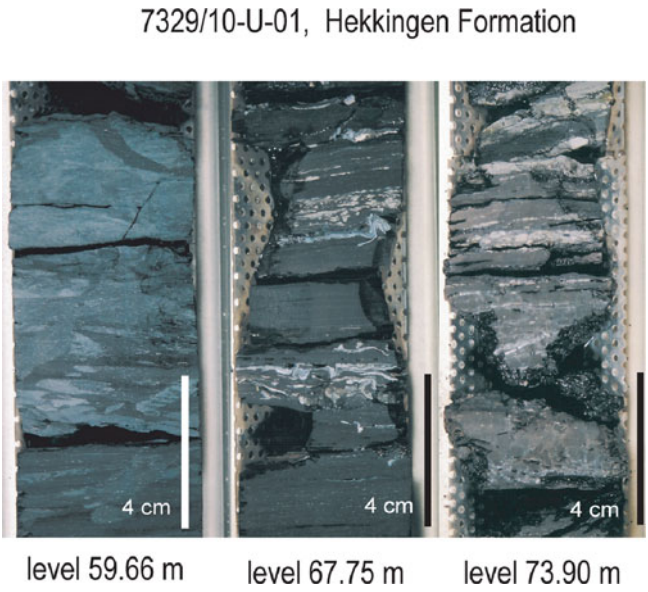

Fig. 5.12 Core photos of Hekkingen Formation; the *left* show bioturbated grey shales, the *middle* one show finely laminated black shales with macrofossils, while the *right photo* show the black shales with this, distal turbidite laminae (sedimentological logs in Figs. 5.2 and 5.8)

Table 5.1). The three thickest conglomerate beds consist of mainly dispersed subangular to subrounded clasts (Fig. 5.8). These clasts are in thin section seen to be composed predominantly of greyish dark brown clay- and siltstone with few sandstone clasts (Fig. 5.10). The texture is most commonly grain-supported with a poorly sorted grey, silty to clayey sandy matrix and a few dispersed *Tasmanites* algae. Sorting is poor to moderate and clasts are distributed throughout the bed, whereas a grain-supported appearance increases near the top. The clasts are commonly around 3 mm in size and mainly randomly oriented. The largest clast found was a 4 cm long sandstone pebble. Rare brown colored sandstone clasts show light greyish-brown coloured alteration rims, whereas no comparable rim has been observed in the much more common grey clasts (Fig. 5.10).

Thinner sandstone beds occur in between the conglomeratic beds. These are generally well sorted and decrease in grain size upwards, forming an overall fining-upwards succession. The sandstones show parallel lamination and rare cross-bedding, typical for tractive sediment transport. These conglomerates and sandstone beds are interpreted as turbidite and debris flow beds based on grain size and sorting, as well as on clast- and matrix-support (Figs. 5.8 and 5.9). Such density flows may have been formed along the central peak and the crater rim, representing the late modification or early postimpact phase of the crater (Dypvik et al. 2004c).

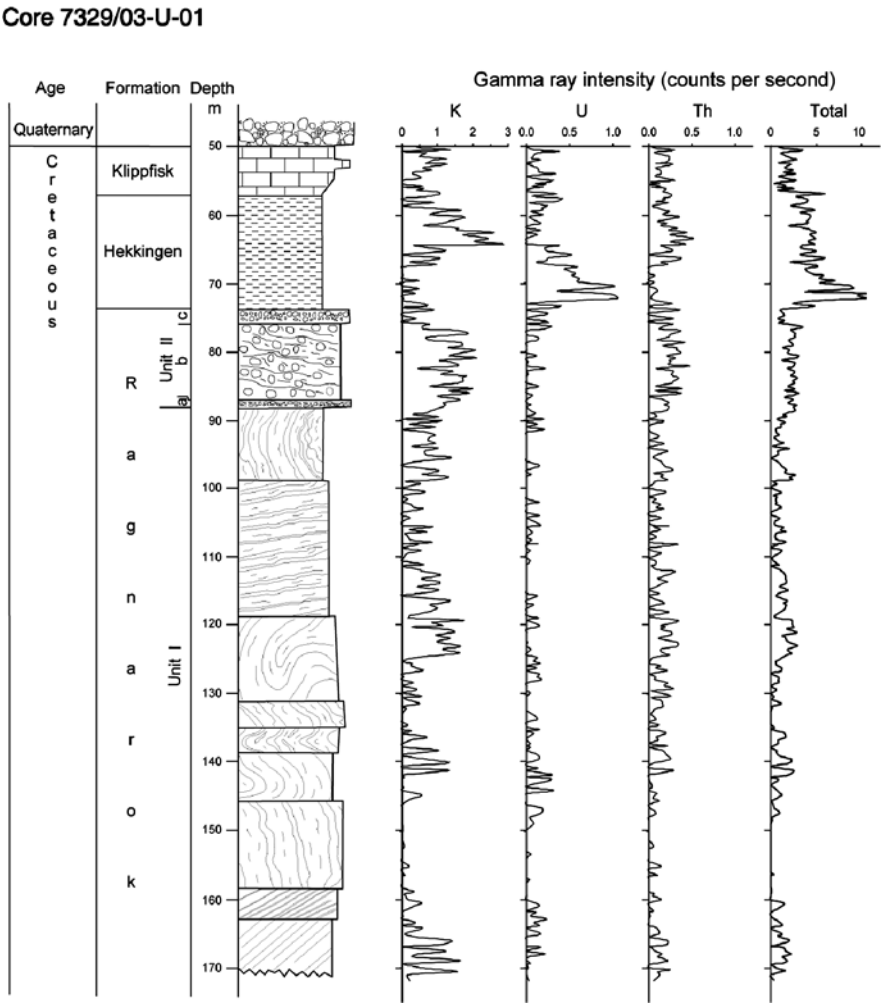

Fig. 5.13 Total gamma log of core 7329/03-01, along with the K, U and Th contributions

The samples have been analysed by standard total organic carbon (TOC) and Rock Eval analysis. Rock Eval is a standard pyrolysis method for source rock characterization and evaluation (Espitalié et al. 1977). In the pyrolysis the measured hydrogen index (HI) (mg hydrocarbons/g organic carbon) and oxygen index (OI) (mg CO_2/g organic carbon) characterizes the kerogen: high HI values (> 100) are typical for good petroleum source rocks. The organic maturity is measured by the T_{max} value in the Rock Eval analysis: the temperature when hydrocarbon production is at its highest in the pyrolysis (Espitalié et al. 1977). The total organic carbon (TOC) content and Rock-Eval hydrogen index values (HI) of the rocks from subunits

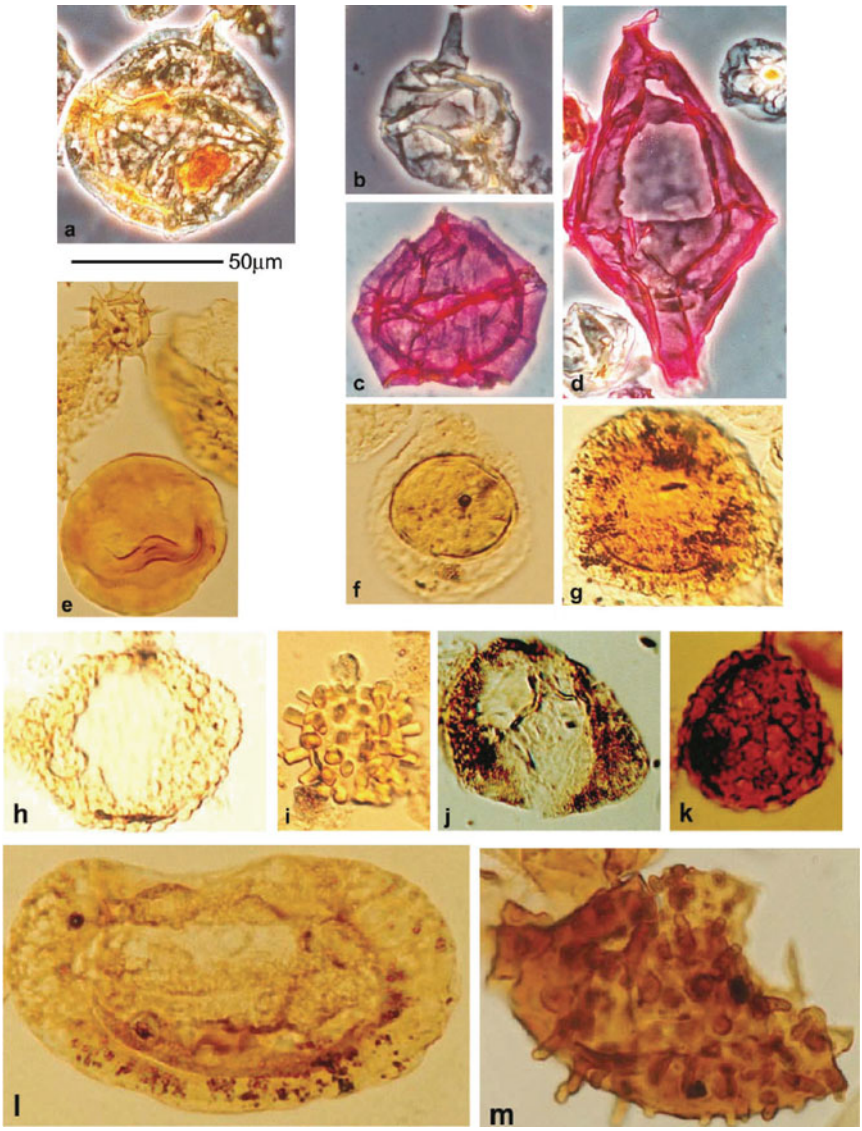

Fig. 5.14 Palynomorphs found in Ragnarok Formation of core 7329/03-01. The 50 µm scale indicates the enlargement of the palynomorphs. Details and references for the different palynomorphs can be found in Fig. 13 in Dypvik et al. (2004b): **(a)** *Cribroperidinium globatum*, **(b)** *Pareodinia ceratophora*, **(c)** *Sirmiodinium grossii*, **(d)** *Tubotuberella*, **(e)** *Tasmanites* sp. and *Microhystridium* sp. (*the upper left corner*), **(f)** *Aulisporites astigmosus*, **(g)** *Doubingerispora filamentosa*, **(h)** *Protodiploxypinus macroverrucosus*, **(i)** *Echinitosporites iliacoides*, **(j)** *Triadispora obscura*, **(k)** *Rewanispora foveolata*, **(l)** *Illinites chitonoides*, and **(m)** *Jerseyiaspora punctispinosa*

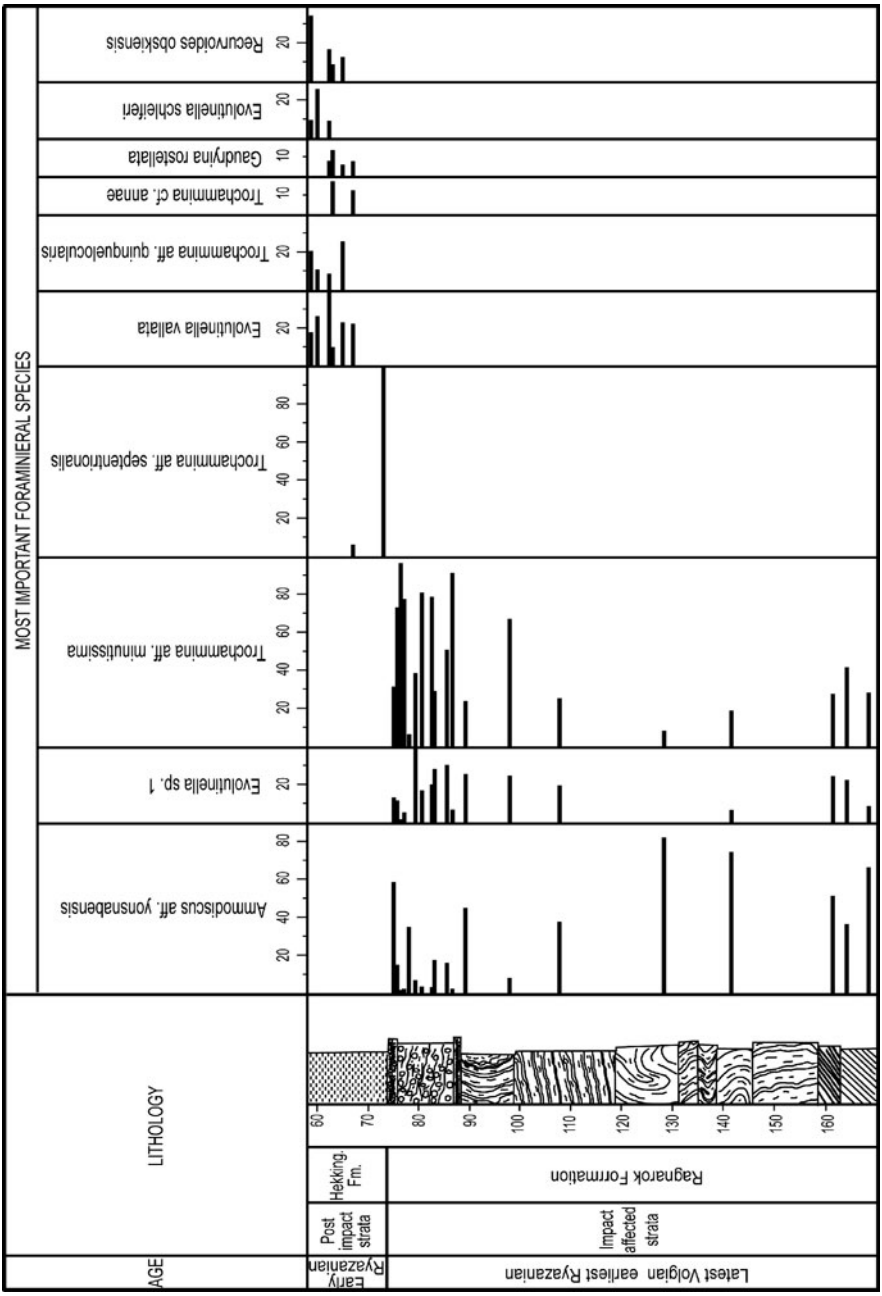

Fig. 5.15 The most important foraminiferas found in core 7329/03-01 (Bremer et al. 2004)

Table 5.2 Geochemical data from the Barents Sea. TOC analysis (weight %) and Rock Eval analysis of core 7329/03-U-01. Sample number is m in depth below sea floor. According to Ohm et al. (2008), the average lower Hekkingen contain 9.7 weight % TOC and HI of 303, while the upper Hekkingen contain 4% TOC and HI of 288

Core 7329/03-U-01				
Sample (m depth)	TOC %	T_{max} °C	HI mgHC/g C	OI $mgCO_2/gC$
58.5	2.03	421	125	4
59.5	7.13	420	446	4
60.6	8.17	416	505	12
61.5	9.98	425	539	7
62.5	3.33	421	276	5
63.5	4.06	420	291	4
64.5	6.89	418	455	6
65.5	4.00	415	298	4
66.5	18.42	412	504	5
67.5	23.24	410	449	4
68.5	21.18	425	591	2
69.5	21.07	419	351	4
70.5	22.12	416	500	3
71.5	25.48	417	522	4
72.5	16.84	420	504	3
73.5	20.21	424	547	4
74.5	0.63	428	51	22
75.5	4.46	427	328	6
76.5	1.67	434	327	10
77.5	1.50	422	63	5
78.5	1.32	434	104	7
79.5	1.19	438	146	87
80.5	1.11	437	120	152
81.5	1.18	437	121	133

IIb and IIc vary, but are much lower than in the overlying shales of the Hekkingen Formation (Table 5.2) (TOC: 0.6–4.5 wt%, average 1.6 wt%; HI: 51–328 mg/g TOC, average 130 mg/g TOC). The T_{max} values vary from 422°C to 439°C, and are on average about 10°C higher than in the Hekkingen Formation samples (432°C vs. 422°C). This may suggest that the Hekkingen Formation contributed only to minor amounts of reworked sediments to the Ragnarok Formation. This assumption is also supported by the sparse recovery of dinoflagellate cysts from the pre-impact Hekkingen Formation in this unit (i.e., only at levels 89.11, 88.20 and 97.93 m).

5.2.4 Hekkingen Formation

In the Mjølnir crater core the Hekkingen Formation comprises black to medium grey, organic rich and laminated shales (74.05–57.10 m; Figs. 5.3, 5.8, 5.11, and 5.12). The bivalve *Buchia* is abundant throughout the formation, and some

specimens have even preserved their nacreous aragonite inner coatings. The shales contain abundant pyrite concretions (0.2–2 cm) and occasionally pinkish brown siderite concretions. The lithology is similar to that of the upper part of the same formation in the neighbouring core 7430/10-U-01 (Fig. 2.12) and elsewhere in the Barents Sea (Worsley et al. 1988; Leith et al. 1992) (Figs. 5.3, 5.8, 5.11, and 5.12).

The interval from 73.89 to 73.78 m contains six thin conglomeratic layers, only from 5 cm to less than 1 cm thick (Figs. 5.8 and 5.12). They are clast-supported and typically display a sharp, erosional base. The conglomerates contain dark grey clasts reworked from Hekkingen Formation shales, and clasts of a lighter grey colour, which have a composition similar to those in the conglomerates of unit IIc of the Ragnarok Formation.

The interval between 73.78 m and the top of the Hekkingen Formation (57.10 m) is dominated by parallel laminated shales. These are dark grey up to about level 68 m and lighter grey in the remaining upper part of the interval (68–57.10 m) (Fig. 5.12). Thin sections display remnants of Prasinophytae algae *(Leiosphaeridia,* 20–50 μm in diameter) and enrichments in *Buchia* shell-fragments. Between 65 and 63 m no macrofossils were found, but they are again present in the upper part of the Hekkingen Formation from 63 to 57.10 m. Trace fossils (dominantly *Chondrites* and *Planolites)* and carbonate concretions are common at different levels in the upper part of the interval. Based on the macrofossils the post-impact Hekkingen Formation is dated as latest Volgian to earliest Ryazanian (Smelror et al. 2001a, b).

The organic matter is thermally immature, as seen in Rock-Eval, T_{max} values of typically 420°C–432°C (Tables 5.2 and 5.3) and production index (S1/(S1 + S2)) values typically less than 0.05. The uranium distribution curve derived from spectral gamma ray measurements (see below) shows a maximum at 67–74 m depth and correlates with the organic richness (Tables 5.2 and 5.3, Fig. 5.13). The total organic carbon (TOC) content in the lower, laminated part of the Hekkingen Formation varies between 17 and 34%, which is similar to, and partly exceeds, the organic richness reported for this formation elsewhere in the northeastern Barents Sea (e.g., Leith et al. 1992; Bugge et al. 2002). High TOC values and hydrogen index values of 351–715 mg/g TOC indicate that the kerogen belongs to mostly type II and locally type I, deposited in an anoxic environment. Spectral gamma values for uranium in the upper part of the section (~68–57.10 m) are rather low.

Organic richness and hydrogen index of these rocks are more variable and generally lower than in the underlying interval (1.1–21.6 wt% TOC, HI = 49–574 mg/g TOC) (Tables 5.2 and 5.3). This is consistent with a less oxygen-deficient depositional environment as suggested by the variable, generally lighter colours and the occasional bioturbation of these shelf deposits.

5.2.5 Klippfisk Formation

The 7.1 m thick interval representing the Klippfisk Formation consists of heavily bioturbated, light greenish-grey, argillaceous carbonates (marls) (Figs. 5.2 and 5.3). The lithology is similar to that of the Klippfisk Formation in type well 7430/10-U-01, described by Smelror et al. (1998) as representing a condensed carbonate

Table 5.3 Geochemical data from the Barents Sea. TOC analysis (weight %) and Rock Eval analysis of core 7430/10-U-01. Sample number is m in depth below sea floor. According to Ohm et al. (2008), the average lower Hekkingen contain 9.7 weight % TOC and HI of 303, while the upper Hekkingen contain 4% TOC and HI of 288

Core 7430/10-U-01				
Sample (m depth)	TOC %	T_{max} °C	HI mgHC/g C	OI $mgCO_2/g$ C
45.1	12.90	420	517	14
45.3	7.52	424	537	13
45.4	3.90	424	288	12
45.6	2.15	423	174	14
45.7	2.99	425	218	10
45.9	6.48	421	392	12
46.2	2.88	422	305	28
46.3	5.45	419	330	11
46.6	17.90	416	462	13
46.8	16.40	416	456	12
47.0	19.80	416	300	10
47.4	9.13	421	491	11
47.5	4.07	421	389	13
47.6	5.30	415	235	16
47.8	17.70	426	572	8
48.2	15.40	415	314	10
48.4	13.60	419	510	8
48.5	27.80	423	451	8
48.6	13.30	425	496	7
48.9	19.60	423	423	8
49.1	17.10	425	497	8
49.2	7.72	421	306	11
49.4	15.50	425	467	7
49.5	14.30	424	446	8
49.6	15.00	422	350	8
49.9	16.70	425	475	8
50.0	23.40	422	319	7
51.0	13.80	419	374	10
52.0	12.10	419	338	12
52.5	18.30	420	330	11
52.9	16.00	417	321	12
53.5	8.91	413	317	14
53.7	10.00	414	323	14
54.0	8.89	417	377	15
54.5	6.03	412	274	22
55.0	5.50	418	294	22
55.3	6.39	418	194	21
55.5	6.21	417	284	21

platform. The top of the formation is not preserved at this locality in the Mjølnir crater as the overlying Quarternary till rests directly on the marls of the Klippfisk Formation.

5.2.6 Spectral Gamma Results

Natural spectral gamma radiation (K, U, Th, total gamma) was measured on the core in the laboratory (Fig. 5.13). Both the total gamma and the spectral gamma readings for the Klippfisk and Hekkingen formations in core 7329/03-U-01 are similar to those found in the neighbouring core 7430/10-U-01. The total gamma measurements in the cored Ragnarok Formation are significantly lower than those of the Hekkingen Formation, and the spectral intensities for uranium are close to the detection limit. Uranium is known to be associated with anoxic depositional conditions and organic material. Gamma readings in homogeneous lithologies therefore commonly correlate with variations in the contents of organic matter (e.g., Supernaw et al. 1978; Schmoker 1981; Fertl and Rieke 1980; Dypvik and Eriksen 1983; Dypvik 1993). The low uranium gamma values in the Ragnarok Formation suggest that the Hekkingen Formation, which was still unconsolidated when the impact occurred, contributed little sediment to the Ragnarok Formation, in agreement with the palynological observations (see below). In the target area most of the Hekkingen Formation was blown away or went up in fire (Dypvik et al. 2008b).

The pronounced increase in K-activity at 65 m in the Hekkingen Formation may reflect a decrease in smectitic fractions and an increase in illitic components (Fig. 5.13). This is also indicated by Dypvik et al. (2003), who demonstrated an increased in the illite content in the one sample (60.00 m) they analyzed from the Hekkingen Formation interval shallower than 65 m.

5.2.7 Paleontology of the Ragnarok Formation

The marine macro- and microbiotas of core 7329/03-U-01 have been described by Smelror et al. (2001b, 2002), Bremer et al. (2004), Dypvik et al. (2004b) and Smelror and Dypvik (2005, 2006).

Below follows an overview of the palyno-flora found in the Ragnarok Formation. The main purpose of these analyses has been to document the ages of the rocks from which the impact breccia was derived. Altogether 117 palynomorph taxa have been recognized in core 7329/03-U-01. Palynomorphs derived from terrestrial sources dominate and indicate that the formation comprises rocks of different ages. Figure 5.14 present some of 39 stratigraphically important taxa.

Only age-significant taxa are commented in the following:

- *Illinites chitonoides* and *Jerseyiaspora punctispinosa,* which occur regularly, range in age from the Late Spathian to the Carnian. *J. punctispinosa* is restricted upwards to Middle Anisian deposits. Both *Densoisporites nejburgii* and *Rewanispora foveolata* have ranges restricted upwards to the Lower Anisian deposits (Fig. 5.14).
- *Aratrisporites macrocavatus* and *Conbaculatisporites hopensis* are characteristic for the Upper Anisian to Ladinian of the Sassendalen Group on the Svalis

Dome. On Svalbard these taxa continue into the Carnian of the Kapp Toscana Group (J.O.Vigran, unpublished data). Bjærke and Manum (1977) illustrate them from Hopen and Kong Karls Land (Kapp Toscana Group; De Geerdalen and Wilhelmøya formations).

- *Echinitosporites iliacoides* is restricted to the Ladinian on Svalbard and the Barents Sea Shelf (Vigran et al. 1998). *Ovalipollis pseudoalatus*, *Schizaeoisporites worsleyi* and *Sellaspora rugoverrucata* have been recorded from the Lower Ladinian on Svalbard and the Barents Sea Shelf, Svalis Dome (Vigran et al. 1998).
- An Upper Ladinian-Lower Carnian association is recognized on the basis of *Aulisporites astigmosus*, *Camerosporites secatus*, *Chasmatosporites major*, *Doubingerispora filamentosa* and *Paracirculina tenebrosa*. It should, however, be noted that most of the evidence described by Bjærke (1977) and Bjærke and Manum (1977) from the Upper Triassic deposits of Hopen and Kong Karls Land has not been recorded in this core.
- *Cerebropollenites macroverrucosus* has the oldest appearance in lower Lower Jurassic rocks. Poorly preserved specimens recorded as Lower Jurassic dinocysts (Fig. 5.14, Nos 16–23) confirm that Lower Jurassic deposits are represented throughout the Ragnarok Formation.

The palynomorph content suggests that the scree and slump complex of sediments forming the Ragnarok Formation in core 7329/03-U-01, interval 170.94–89.11 m (most of unit I) have their major source in the Middle Triassic deposits of the Sassendalen Group. Some of the palynomorphs probably represent the Lower Carnian, i.e., the oldest deposits of the Wilhelmøya Subgroup, but there is no palynological evidence allowing recognition of a Carnian-Norian association of the Kapp Toscana Group. Lower Jurassic palynomorphs are generally only present in minor proportions.

Samples at 88.20–77.80 m, representing the uppermost part of the Ragnarok Formation (uppermost part of unit I, subunits IIa and most of subunit IIb) contain a stratigraphic mixture of pollen and spores from the Middle to Upper Triassic and Lower Jurassic. The dominance of *Botryococcus* and marine plankton of presumed Jurassic age distinguishes these samples from those in the lower part of the core, containing dominantly terrestrial material.

One sample at 86.20 m contains dinoflagellate cysts of late Middle to early Late Jurassic affinity (i.e., *Dichadogonyaulax* sp. and *Chytroeisphaeridia hyalina*). Three samples from 89.11, 88.20, and 87.93 m include Late Jurassic dinoflagellate cysts in addition to the Late Triassic to Early Jurassic terrestrial palynomorphs. Characteristic species found in these samples are *Atopodinium haromense, Paragonyaulacysta borealis, Cribroperidinium* spp. (including *C. globatum*), *Senoniasphaera jurassica,* and *Tubotuberella apatela.* They are derived from the pre-impact deposits of the Hekkingen Formation.

The foraminiferal zonations are displayed in Fig. 5.15 (Bremer et al. 2004), which are presented in more detail in Sect. 5.4.5.

5.2.8 Paleontology of the Hekkingen Formation

Overlying the Ragnarok Formation there are 17 m dark shales of the Hekkingen Formation. The Hekkingen Formation contains a low-diversity macrofauna with species of the bivalve genus *Buchia*, and low diversity assemblages of palynomorphs and microfossils (Smelror et al. 2001b, 2002; Bremer et al. 2004; Smelror and Dypvik 2005, 2006).

The most prolific feature of the post-impact sediments in the Mjølnir crater core is the very distinct bloom of the prasinophycean alga *Leiosphaeridia* in the oldest post-impact sediments of the Hekkingen Formation. This impact-induced algal bloom is described in more details in Sect. 5.4.5.

At the base of the post-impact succession *Buchia unschensis* appears at 73.97 m (Smelror et al. 2001a, b). It is the first identifiable species to occur above the disturbed strata of the Ragnarok Formation and therefore is most important for identifying the date of return to normal sedimentary conditions after the Mjølnir impact. Specimens of *Buchia unschensis* are found at several levels upwards in the core, with the uppermost occurrence at 67.14 m. According to Zakharov et al. (1981), the *Buchia unschensis* Zone can be correlated to the upper part of the *Craspedites okensis* and the lower part of the *Chetaites sibericus* ammonite zones in Siberia. In North Greenland, *Buchia uschensis* is found in strata of the *Crappedites okensis* to *Hectoroceras kochi* ammonite zones and in East Greenland from the *Virgatosphinctes tenuicostatus* to *Hectoroceras kochi* zones (Surlyk and Zakharov 1983). *Buchia unschensis* has also been recovered from the *Craspedites nodiger* ammonite Zone (Yershova 1983).

Further upwards in the Mjølnir crater core *Buchia okensis* is found between 66.80 and 60.13 m. This species is known to range from the upper part of the *Chetaites sibericus* ammonite Zone to the *Bojarkia mesezhnikowi* Zone in the central part of the Russian Platform (Zakharov 1981). *Buchia okensis* is also known from the Ryazanian of Spitsbergen (Yershova 1983).

At 60.37 m in the Mjølnir crater core 7329/03-U-01 an ammonite identified as *Borealites* sp. has been described (Smelror et al. 2001a). This species is closely comparable to *Borealites* sp. aff. *fedorovi* as illustrated by Håkansson et al. (1981) from the Early Ryazanian *Hectorocera kochi* ammonite Zone of Peary Land on Northern Greenland.

The present biostratigraphic evidence from the Mjølnir crater core supports the data from borehole 7430/10-U-01 that the oldest post-impact sediments correspond in age to the uppermost Volgian – lowermost Ryazanian *Buchia unschensis* Zone. The age-range of this zone corresponds to the *Subcraspedites primitivus* to *Runctonia runctoni* ammonite zones of the standard Boreal succession (Rawson et al. 1999).

The marine microfloras found in the post-impact Hekkingen Formation of the Mjølnir crater core are described in details by Smelror and Dypvik (2005). The marine microfloras of the oldest post-impact deposits (74.05–64.9 m) are totally dominated by the *Leiosphaeridia* bloom, while dinoflagellate cysts are most common in the overlying deposits of the Hekkingen Formation (64.9–58.5m). The

diversity of marine microplankton is relatively moderate throughout the formation, varying from 4 to 18 species per sample. Few age-diagnostic species are recovered, but the presence of *Gochteodinia villosa* at 62.0 m allows a correlation to the *Gochteodinia villosa* (Gvi) Interval Biozone of Riding and Thomas (1992). The Gvi-zone spans the Portlandian to Ryazanian in the British Jurassic.

5.2.9 Magnetic Properties and Densities of the Mjølnir Crater Core (7329/03-U-01)

Here we present measurements of magnetic properties and densities for two sample sets. Susceptibilities were measured using a Bartington MS2c sensor in a core-scanning set-up. Sampling was limited by the physical condition of the core, as the instrument set-up requires intact core-sections of at least 10 cm in length. For this sample-set only total susceptibilities were measured (Fig. 5.16). The second dataset consists of selected samples investigated in a laboratory environment (Torsvik and Olesen 1988), and both volume-specific susceptibilities and densities were determined (Fig. 5.16). Susceptibility values ranged between zero (i.e., below the instrument noise level) and 200×10^{-5} SI, common values for marine sedimentary rocks. The sample selection is biased to competent samples. Overall, maximum susceptibility values are found in samples with rusty colours. Typical magnetic sources in such a sedimentary environment aside the bedrock are deposited detrital magnetic minerals and siderite-cemented beds or nodules aside.

The measured densities range between 1,500 and 2,900 kg/m^3 and mostly around 2,400 kg/m^3 (Fig. 5.16). This selection is also biased to more competent core sections because of the density measuring procedure, i.e., the "Archimedes" principle that does not allow measurements of unconsolidated sediments. The densities determined here are dry densities, because any persistent exposure to water would have dissolved most samples. The two extreme end-members are related to materials such as coal (sample 12) or siderite nodules (sample 6). Generally, the densities increase with depth likely due to compaction. During the drilling, the first 60 m were penetrated without recovering the core. These first layers are unconsolidated Quaternary sediments, which have densities less than 1,700 and as low as 1,300 kg/m^3. Following the density measurements of the core samples, densities for the uppermost layers of the subsurface model of Mjølnir were derived and are plotted in Fig. 5.16.

5.3 The Mjølnir Impact Event in a Sequence Stratigraphical Framework

The Mesozoic formations can be correlated in detail across the Arctic, and within the Jurassic and Cretaceous several stratigraphical sequence boundaries can be followed (Mørk and Smelror 2001), as already discussed in Chap. 2. Embry (1989) presented

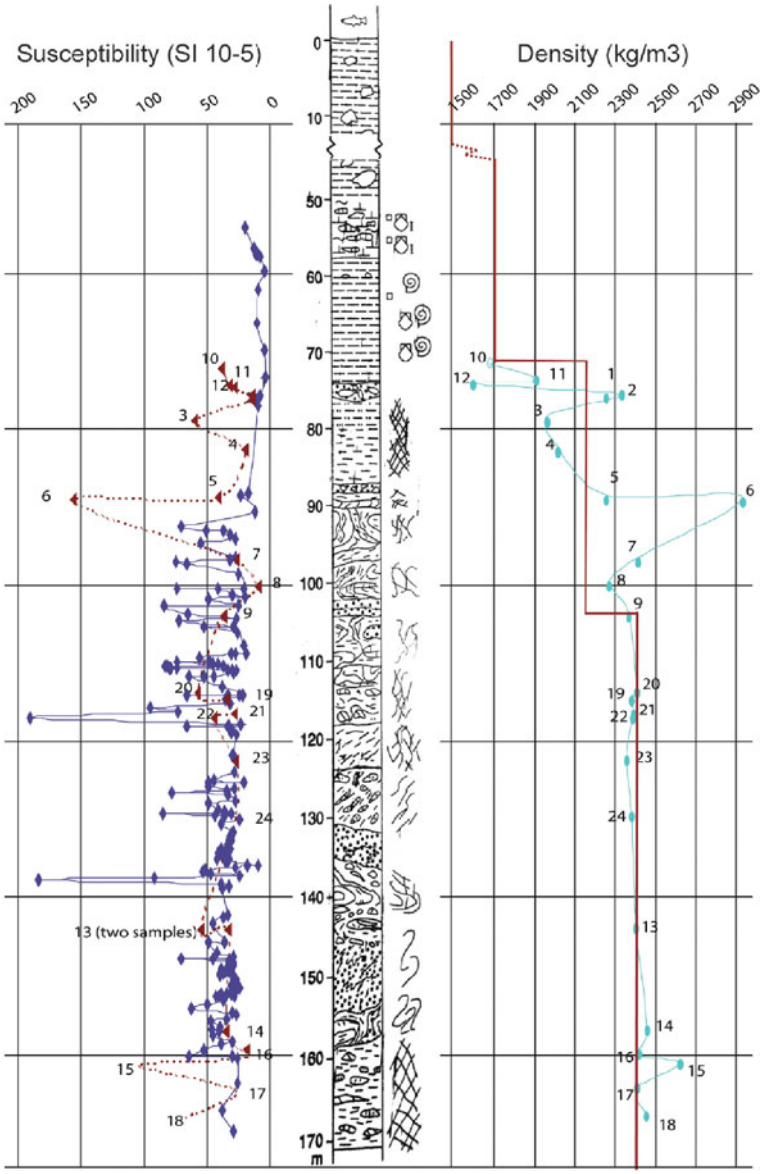

Fig. 5.16 Stratigraphy of core 7329/03-U-01 (Mørk, personal communication 2006) and measurements of susceptibilities (*left*) and densities (*right*) of competent samples. The *red curve* indicates the density variations with depth as used for the *upper* most layers of the density model. Degrees of fracturing and folding indicated in- and along the central sketched geological column

the Carboniferous to Tertiary correlation across the Arctic, through numerous unconformity bound sequences. Whether this correlative development is due to tectonics or eustasy will have to wait for further research. Embry (1989) claims tectonic influence to be of major importance in the Mesozoic of the Arctic. In this chapter we will take a closer look at the Jurassic and Cretaceous sequences.

The Janusfjellet Subgroup of Svalbard can be correlated to the Mackenzie King Group of the Sverdrup Basin including the Oxfordian Ringnes Formation, Kimmeridgian Awingak Formation and Valanginian Deer Bay Formation (Fig. 5.17). The lowermost boundary of the Janusfjellet Subgroup falls within the Middle-Late Bathonian, while the sands of the Oppdalsåta Member (about Kimmeridgian) correlates fairly well with the Awingak Formation of the Sverdrup basin and a well defined lower unconformity at 153 Ma. The boundary between the Jurassic Agardhfjellet Formation and the Early Cretaceous Rurikfjellet Formation is located at the 143 Ma unconformity. This sequence boundary has been identified in the Canadian Arctic as corresponding to the boundary between the Awingak and Deer Bay formations (Embry 1989). As presented in an earlier chapters, the Svalbard and the Barents Sea successions can be correlated fairly well (Mørk et al. 1999) (Figs. 1.3, 2.5 and 5.17). The Bathonian to Volgian successions of the southwestern Barents Sea belong to the lower part of the Adventdalen Group (Fuglen and Hekkingen formations) and are also dominated by very fine grained sediments disclosing two lower transgressive and an upper regressive development (Mørk and Smelror 2001; Smelror et al. 2001a, b). The uppermost boundary of the Adventdalen Group is marked by a short and subtle regressive trend just before the sequence boundary between the Berriasian and Valanginian successions. This marks the boundary between the Hekkingen Formation (Krill Member) and the Klippfisk Formation (Smelror et al. 1998; Fig. 5.17).

In the Harstad Basin, Smelror et al. (2001b) demonstrated a transgressive development from Bathonian to Oxfordian. This so-called Callovian transgression (Bathonian-Oxfordian) has also been recognized on Svalbard (Dypvik et al. 1992). The Lower Oxfordian sequence boundary (159 Ma) on top of the Callovian transgressive beds forms the base of the Hekkingen Formation, which includes the black shales of the Alge Member in its lowermost part. The Alge Member contains organic matter type II and III and represents deep shelf, anoxic depositional conditions (Leith et al. 1992). The Alge Member (Oxfordian to Kimmeridgian) was described by Smelror et al. (2001b) to demonstrate the expanding puddle mechanism (Wignall and Hallam 1991) in a transgressive development. The succeeding upper part of the Hekkingen Formation represents a regressive phase. Wierzbowski et al. (2002) studied the Upper Oxfordian to Kimmeridgian in Nordland VII area to the south of Barents Sea; focusing in particular on the ammonite and dinoflagellate faunas. The studied units from Nordland VII show the same transgressive developments and can be stratigraphically tied to the Barents Sea, Svalbard and East Greenland (Fig. 1.3).

The uppermost part of the Hekkingen Formation is made up of the Krill Member, which generally represents anoxic to dysoxic deep shelf conditions with a mixture of terrestrial and marine organic matter (Leith et al. 1992). The greenish, partly nodular marls of the Klippfisk Formation represent deposits from local highs with reduced

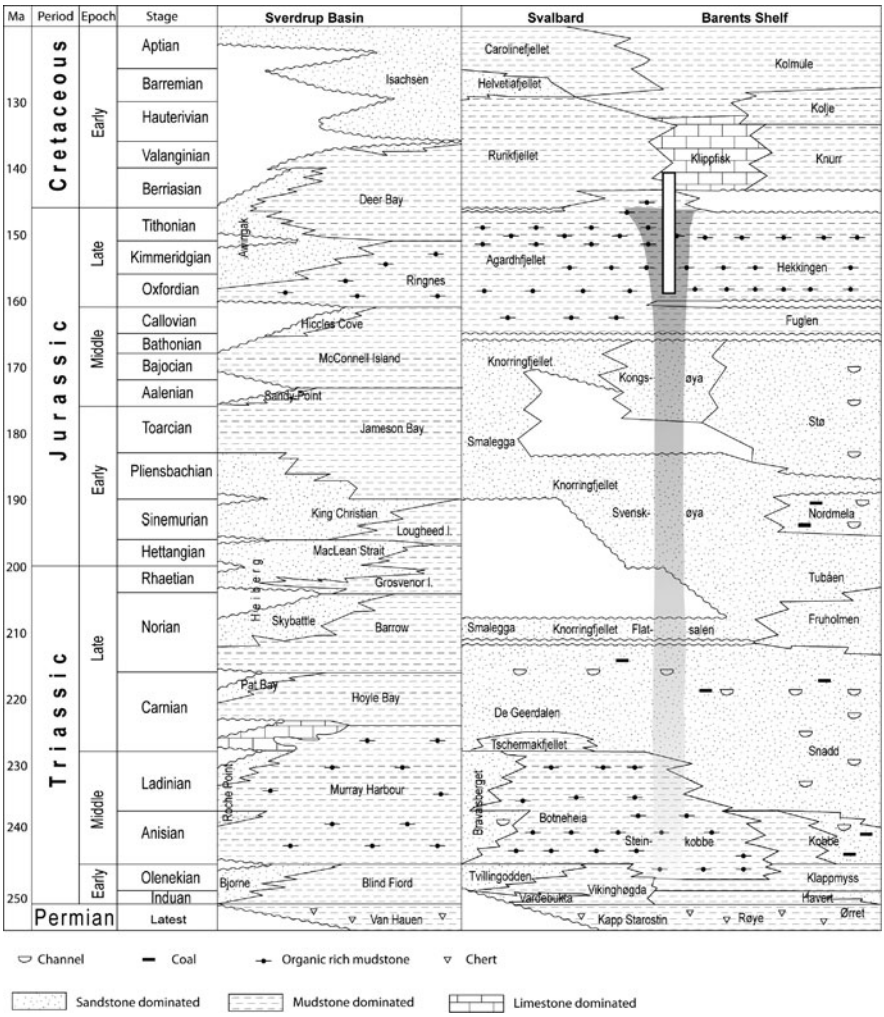

Fig. 5.17 The correlation scheme illustrates the stratigraphical correlation in the Arctic between the Sverdrup Basin (Canada) and the Barents shelf region. The Mjølnir crater erosinal cut is illustrated, while the *white*, *solid block* (Mjølnir core) indicates that only the upper part was drilled. The *shadowed area* displays that the ejected/reworked crater material found in the breccias of the crater core are dominately by Triassic and early to mid Jurassic age clasts. Fossils from ejecta material indicate disturbance down to the Lower Triassic, while the Permian-Triassic bounday was not penetrated. The Figure is base on Embry and Beaucamp (2008), Mørk et al. (1999) and Mørk and Smelror (2001)

clastic sedimentation and increased biological production in the Barents Sea region (Smelror et al. 1998, 2001b). This Lower Cretaceous unit is confined by a sequence boundary succeeded by the dark claystones of the Kolje Formation. Further, into the Cretaceous, the basin development was characterized by improved ventilation in the water masses and fading out of the anoxic/dysoxic domain.

In the Svalbard succession (Fig. 5.17) details in the transgressive Late Jurassic (Oxfordian-Early Volgian) development was demonstrated by Dypvik et al. (1992) in a study of the Myklegardfjellet Bed (the lowermost part of the Rurikfjellet Formation) and its adjacent formations. They found the major Volgian part, i.e., the latest Jurassic to display a regressive trend into the Myklegardfjellet Bed at Svalbard, which after a thin and fine-grained transgression, develops into the well known regressive Lower Cretaceous succession composing the main body of the Rurikfjellet Formation (Worsley et al. 1988). This development was later partly recognized in the Barents Sea successions by Smelror et al. (2001b), as stated above. In the Svalbard succession, just below the Myklegardfjellet Bed, the Mjølnir impact is indicated by ejected material recognized in the Janusfjellet succession (see Chap. 6). The Late Jurassic regressive development (about 143–142 Ma) is of more regional/global character. Smelror et al. (2002) displayed the Mjølnir impact effect to be reflected in the palynoflora of the region by possible renewed circulation in the water masses and temporarily increased supply of nutrients. This is demonstrated in the prolific bloom of *Leiospheridia* (green algae) and *Botryoccoccus* (fresh water algae) over wide areas in the southern Barents Sea and Svalbard. These blooms occur at the same time as the Ir anomaly, i.e., at the time of impact (Dypvik et al. 2006) (see e.g., Fig. 6.3).

After the Early Cretaceous transgressive period (Dypvik et al. 1992), the Lower Cretaceous regressive development took over. During the Barremian, southeasterly prograding deltas from an uplifted northern region North of Svalbard, moved into the northern part of the paleo Barents Sea (Gjelberg and Steel 1995). This event partly overlaps and strengthens the more regional Early Cretaceous regressive phase. The deltaic progradation across the Svalbard region can be related to local tectonics and uplift along the northern margin of the Barents Sea Region in connection with the opening of the Nansen Basin and spreading along the Gakkel Ridge North (Figs. 2.1 and 2.2).

The Late Jurassic to Early Cretaceous stratigraphical developments outlined above can be correlated with comparable evolution in North Greenland, as exposed in the regions of Kilen and Peary Land (Dypvik et al. 2002; Håkansson et al. 1993) (Figs. 1.3, 2.14, and 2.15). Both the so-called Callovian transgression (Bathonian–Oxfordian) with a maximum extent (flooding?) in Late Kimmeridgian and the following regressive phase are seen (Dypvik et al. 2002; Håkansson et al. 1993; Heinberg and Håkansson 1994). Within the Callovian North Greenland transgressive successions several sand units are present and commonly display coarsening upwards developments (Dypvik et al. 2002).

According to Nagy et al. (1988) and Dypvik et al. (1992) the Ryazanian flooding succeeding the Myklegardfjellet Bed on Svalbard (Fig. 1.3) can be interpreted to represent a maximum flooding situation. This would be comparable to the middle part of the Krill Member (Hekkingen Formation, Barents Sea), Middle Part of Deer Bay Formation (Sverdrup basin) and lower part of the Dromledome Formation (N Greenland, Figs. 1.3, 2.14 and 5.17).

5.4 The Evidence for Impact Crater Formation

The identification and study of potential impact structures formed by asteroid or comet collisions is complicated, and includes integration of several different types of information in order to achieve the most reliable interpretations. Consequently the identification and presentation of the impact evidences are of great importance and will normally be met with major interest and a large portion of skepticism by the impact community. In this compilation we therefore present some of the main impact evidences we have been able to gather for the Mjølnir structure. For further studies of the more general aspects of these arguments the reader is referred to French (1998) and Montanari and Koeberl (2000).

5.4.1 The Crater: Its Structure and Shape

The first recognition of impact structures is often based on convincing geomorphologic observations of the structure and its more or less circular configuration. Surface structures of circular shape can be formed in several different ways and asteroid and comet impacts are only one of the many explanation alternatives for the circular shapes. Structures with a diameter of 40 km could be formed by, e.g., extensive karstification, halokinesis, volcanic activity, and structural geological activity such as folding. Consequently the identification of a circular structure is not enough, additional evidence is needed.

In the Mjølnir case, the first descriptions and the reconstructions of Gudlaugsson (1993) formed the crucial starting point for further investigations. The structure has been portrayed as a complex crater, 40 km in diameter, with a central high that is 8 km wide along the base, surrounded by a 12 km wide annular basin (Gudlaugsson 1993; Tsikalas et al. 1998a) (e.g., Figs. 3.4, 3.10, and 3.14). A closer description of these characteristics and other geophysical information (e.g., gravimetric and magnetic) is presented in detail in Chap. 4.

The annular basin of the Mjølnir crater has been estimated to have a diameter of 16 km. The dimensions of annular basin and the transient crater, are crucial parameters in understanding crater mechanisms, and are vividly discussed these days (see Turtle et al. 2005). This is in particular the case for complex craters with a brim and an inverted sombrero shape (Melosh 1989), just like the Mjølnir structure (e.g., Figs. 1.10, 3.8, and 3.19). The Mjølnir structure has a peak-ring geometry as should be expected of impact structures larger than 26 km in diameter (Melosh 1989; French 1998). The well preserved peak-ring configuration is additional impact evidence. The excellent preservation of the Mjølnir Crater is the result of an early burial in the marine environment (e.g., Tsikalas and Faleide 2007). The relations between peak height and diameter of the Mjølnir depression are well within the scaling relations of Melosh (1989) (e.g., Tsikalas et al. 1998a–c) (see also Chap. 4).

5.4.2 Fracturing and Conglomerates

In the seismic lines crossing the Mjølnir structure extensive fracturing and brecciation can be observed (Chaps. 3 and 4). This intense fracturing is also highly evident in the Mjølnir core (Figs. 5.3 and 5.16). Several structural phases can be recognized and soft sediment deformation and water escape phenomenon have been demonstrated. This is discussed in detail in Chap. 8. The fracture patterns, observed in the core and of large scale in the seismic lines, display a general circular orientation around the center associated with outwards decreasing intensities. Such observations are very important in impact crater identification (Tsikalas et al. 1998a) and fracture patterns like this have been identified in other impact structures (Chesapeake Bay-Virginia, USA and Neugrund, Estonia). Impact structures may often be deeply eroded and the original fracture patterns can be difficult to detect. In other cases the structural geometry may have been completely eroded, and only remnants of a circular development of brecciaed and partly melted rocks may be present (French 1998).

In the seismic lines and in the few meters of sediment penetrated by the Mjølnir core, several breccias are present (Dypvik et al. 2004b). So-called monomictic authochtonous breccias were formed by crushing the target area and only moving the clasts around locally for short distances. This resulted in a jigsaw puzzle texture, which typically is found in the deeper and central parts of impact craters (French 1998). In a standard impact setting polymict, allocthonous breccias will follow on top of these conglomerates. These polymict breccias are made up of ejected material and sedimentary conglomerates/breccias with clues of traction and sediment transportation (French 1998). In the cores from the Mjølnir Crater only this kind of polymictic breccia were recovered by the drilling, comprising the lowermost part of the Ragnarok Formation (Figs. 5.2 and 5.3). The monomictic authochonous breccias have not been encountered in the Mjølnir core, but most likely make up the deeper central, un-cored parts of the structure. They are most likely represented in the chaotic reflections of the seismic lines in those deeper sections (Tsikalas et al. 1998a–c) (e.g., Fig. 4.4).

Covering the impact breccias, commonly in several craters, glass- and melt-rich formations and so-called suevites follow. They may in turn be succeeded by various sedimentary conglomerates. In the case of Mjølnir no melts or suevites have been found so far, but various types of sedimentary conglomerates are present in the parts of the Ragnarok Formation, while the melt problem of Mjølnir is discussed in the next paragraph.

Shatter cones are a typical structural feature so far only found in impact structures (Montanari and Koeberl 2000). However, no such structures have been found in the Mjølnir core and would be hard to see at such scale.

5.4.3 Mineralogical Evidence of Impact Cratering

Several mineralogical impact indicators have been discovered through the years of impact research (Montanari and Koeberl 2000). The major evidence and most

commonly used mineralogical arguments are fragments of meteorites, shocked minerals (quartz, feldspar, and zircon), high pressure polymorphs (coesite, stishovite), Ni-rich spinels, diamonds, meltphases of various types, including diaplectic glasses and tektites.

In the studies of the Mjølnir impact, analysis of cores from the impact crater, analyses of the ejecta beds and field observations have been carried out. Shocked quartz have been found in both the crater and in the ejecta beds deposited 30 km outside the crater (Sindre Bed), as seen in core 7430 (level 47.6 m see Figs. 6.2 and 6.3) (Dypvik et al. 1996, 2006). The few shocked quartz grains (about 1 by ‰ by number) found in the 7430 core are dominated by PF structures, but also some few PDF have been found (Dypvik et al. 1996; Langenhorst and Dypvik 1996). The shocked quartz from the central part of the structure (Mjølnir core) has been studied and described in detail, with a particular focus on planar microstructures (planar fractures -PF and planar deformation features-PDF) by Sandbakken (2002) and Sandbakken et al. (2005) (Figs. 5.18, 5.19, and 5.20). These shocked grains are dominated by planar fractures and only a few of good planar deformation features have been found (Figs. 5.18 and 5.19). This may largely be attributed to the great difference in compressibilities of the pores and sand grains, resulting in large shear stresses that have been accommodated mainly by fracturing. The different shock features indicate possible formation pressures between 5 and 20 GPa (Fig. 5.20). The samples from the lower part of the core typically show the lowest pressures, whereas the uppermost part of the succession displays the highest pressures, a development comparable to that of the Ries crater (Sandbakken et al. 2005).

In some cases, Ni-spinels (Byerly and Lowe 1994; Robin and Molina 2006), their possible derivatives and even parts of the meteorite may be found (Kyte 2002). In the Mjølnir case we have looked for such impact evidence, but no good examples have been discovered, so far. In a study of samples from Janusfjellet section at Svalbard, Robin et al. (2001) found microscopic grains of nickel-rich iron oxides. These may be remnants of the altered bolide. However, Ni enrichments are commonly found in several of the Upper Jurassic formations, and likely represent enrichments of sulphide phases, mainly demonstrating the consistent anoxic depositional conditions of that time (Dypvik et al. 2006; Dypvik and Harris 2001).

The discussion of impact glass formation, in particular in marine impacts, is going strong within the impact community. It turns out that most marine impact craters are poor in impact melt rocks, and it has been suggested that the production of impact glass normally could be smaller in marine targets (Ormö and Lindström 2000; Dypvik and Jansa 2003). The presence of water results in more violent impacts and possibly more wide-spread distribution of ejecta (Shuvalov et al. 2002; Shuvalov and Dypvik 2004; Tsikalas 2005). So far no impact glass or melt rocks have been found during the detailed petrographic and geochemical studies of the Mjølnir drill-core. In this connection it should, however, be mentioned that the amounts of smectite is rather high in the impact related sediments of Mjølnir (Dypvik and Ferrell 1998, Dypvik et al. 2003). Smectite is regarded to be a most likely alteration product of the impact melt, but it can be formed by several different mechanisms. In this respect the appearance of smectite enrichments can be taken as a weak indication of an original presence of impact glass. No mineralogical or

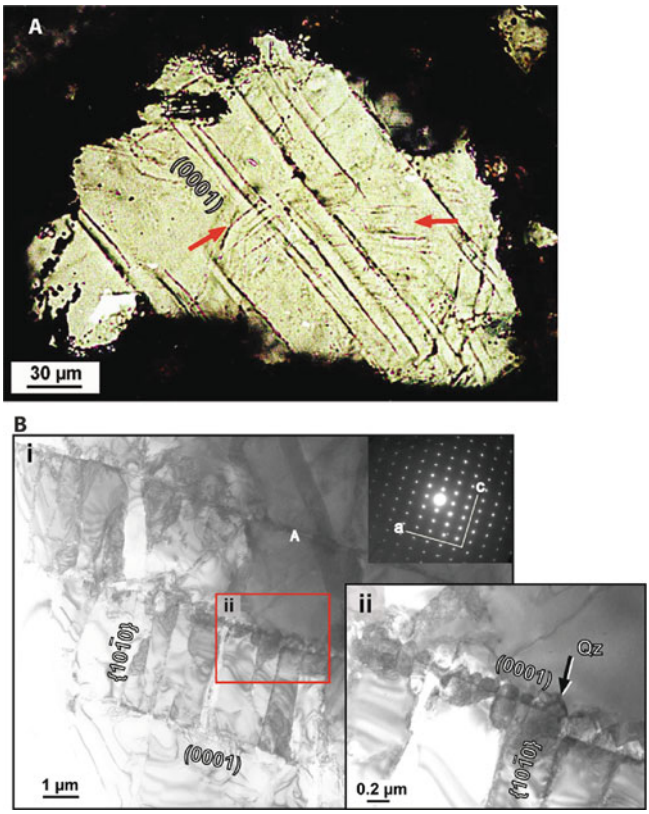

Fig. 5.18 **(a)** (*Upper photo*) Photomicrograph of a shocked quartz grain from unit IIc (74.05 m) with well-developed, irregularly spaced (4–20 µm) PFs (~1 µm broad) parallel to (0001). Two sets of thin (<1 µm) and closely spaced (2–4 µm) PDFs terminate towards the PFs (*red arrows*). On the *left side* of the grain there are indications of chemical etching (plane-polarized light). Shocked quartz grains from 7329. **(b)** (*lower three photos*) Bright field micrograph (TEM) of quartz from unit I (PDF/PF) (100.70 m). (i) Two sets of planar microstructures are shown. The partly open (0001) PFs terminate the thin, sub-planar and sub-parallel {10$\bar{1}$0} PFs. A corresponding diffraction pattern (*inset*) was used to index the planar micro-structures. The *rectangle* (ii) marks the enlarged area in (ii), showing microquartz (Qz) that has crystallized in an open part of the PF (From Sandbakken et al. 2005)

geochemical characteristics of the smectite have, however, been found, which could pin-point an impact related origin.

5.4.4 Geochemistry

Platinum Group Element (Ru, Rh, Pd, Os, Ir, Pt) (PGE) enrichments are well known and commonly used as indications for an impact event (Montanari and Koeberl 2000; Koeberl 2007). In particular Ir and partly Os have been in focus.

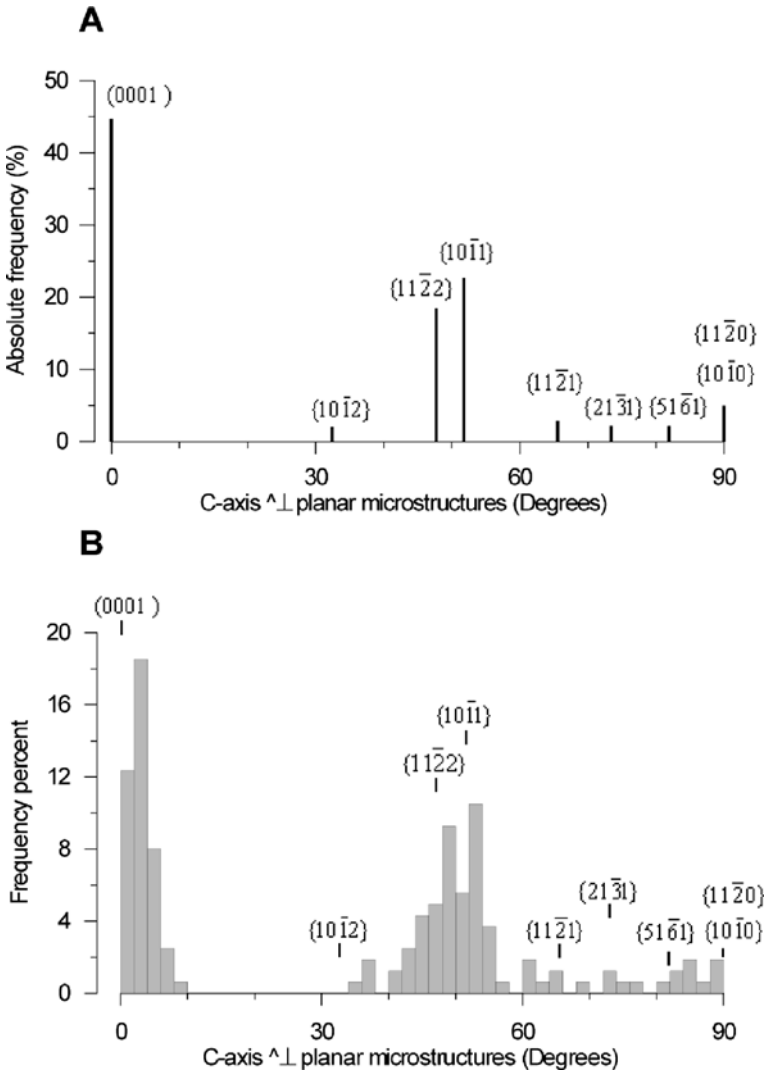

Fig. 5.19 **(a)** Histogram showing the crystallographic orientations of PFs in 100 quartz grains (141 sets, 18% unindexed planes) from core 7329/03-U-01. The planes have been uniquely indexed using a template containing known planar microstructure orientations (From von Engelhardt and Bertsch 1969). **(b)** Histogram showing the angles (binned at 2°) between the c-axis and the poles to PFs. This figure presents similar data as in Fig. 5.19a, but also includes the unindexed planes. Note the analyzed samples represent allochtonous material that represents a mixture of quartz grains recording different degrees of shock (From Sandbakken et al. 2005)

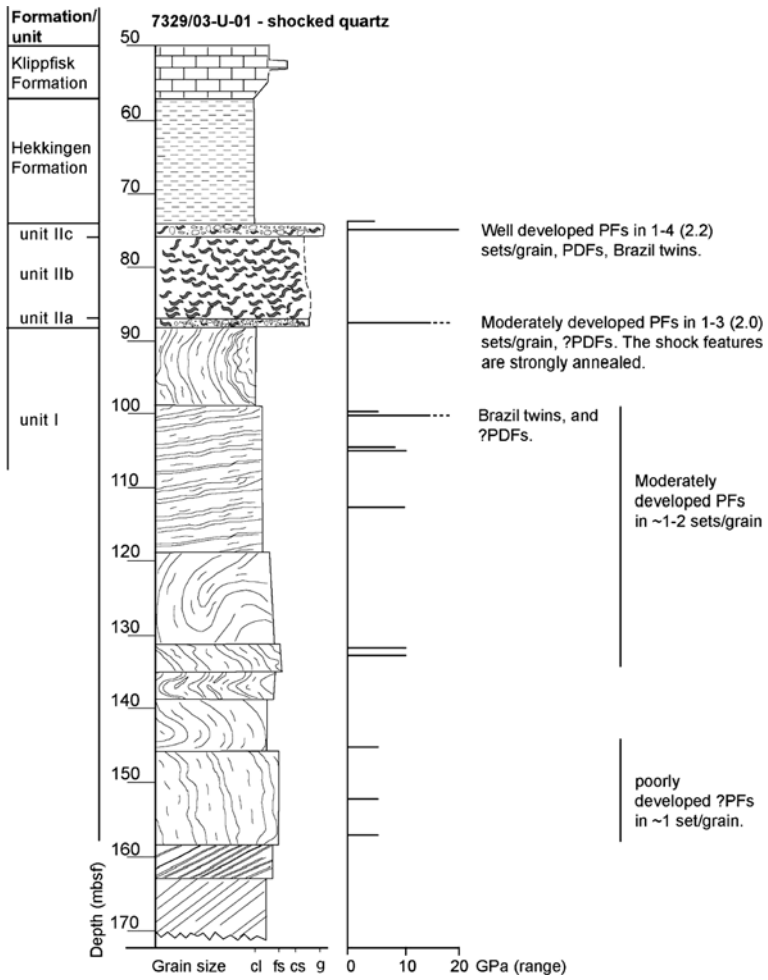

Fig. 5.20 Stratigraphic distribution of shocked quartz in samples from core 7329/03-U-01. The range of shock pressures shown is derived from calibrations on crystalline rocks by shock experiments (Grieve et al. 1996) and should therefore be considered as minimum shock pressures. Mbsf = meter below seafloor. cl = clay, fs = fine sand and silt, cs = coarse sand, g = grain size coarser than sand (From Sandbakken et al. 2005)

In the Earth's crust and surface the Ir concentrations are normally low (20–60 ppt), while Ir enrichments are found in mantle derived rocks. However, not even the largest volcanic eruptions are able to supply high enough Ir-concentrations to the surface in order to match extraterrestrial Ir-supply caused by asteroid and meteorite impacts. In chondrites and iron meteorites several hundred ppb of Ir have been detected (Koeberl 2007). The Ir contents in the samples from the Mjølnir crater core are more than 200 ppt. In the ejecta from drillhole 7430/10-U-01, located 30 km NE

of the crater, a sharp peak of more that 1 ppb has been found (see Figs. 6.2 and 6.3). In this respect it should be mentioned that one sample from Svalbard have been recognized with 2 ppb Ir (Dypvik et al. 2006) at a horizon correlative with the Mjølnir event.

Os- and Cr-isotope analyses can be used in order to confirm the impact origin and a determination of the possible bolide type (Koeberl 2007; Montanari and Koeberl 2000). Recent preliminary Os-isotope analyses of the impact horizon at Janusfjellet, may point towards an iron oxide (possible nickel) rich bolide (S. Graham, personal communication, 2006).

The Cr and Ni distributions have been analyzed in most of the available Svalbard sections and in cores from the Barents Sea region (Dypvik and Attrep 1999; Dypvik et al. 1996, 2006). In the Ir-enriched beds of the 7430 drillhole Dypvik and Attrep (1999) found Ni and Cr values that were interpreted to indicate an iron rich meteoritic composition. This is in agreement with the preliminary Os-isotope results mentioned above and along with the Ni-rich iron oxides discovery from the impact beds at Janusfjellet, Svalbard (Robin et al. 2001). It should be mentioned that mutual Ni and Cr enrichments maybe be partly related to the anoxic/dysoxic deposition conditions at the time of the Mjølnir impact.

5.4.5 Paleontological Evidence of Impact Cratering

The Late Jurassic and earliest Cretaceous on the Barents Shelf were dominated by fine-grained clay sedimentation, with mostly anoxic to hypoxic depositional conditions. The stratified water masses contained typically relatively rich, but low diversity, nektonic faunas and marine microfloras above the pycnocline. In contrast, the benthic faunas contained only a few bivalve species (dominantly *Buchia*) and low diversity communities of foraminifera.

There is no evidence of any major biotic extinction or changes in diversity related to the impact event, but the overall composition of the microfossil assemblages show a significant turnover within the impact influenced strata (Bremer et al. 2004; Smelror and Dypvik 2006). Of particular interest is the previous described sudden bloom of algaes *Leiosphe ridia* and *Botryoccoccus* just after impact and in the same beds with the Ir-enrichments (Smelror et al. 2002; Smelror and Dypvik 2005) (see Fig. 6.3). In the oldest post-impact sediments of the Mjølnir core (i.e., at level 74 m) the acme of *Leiosphaeridia* reach 513,000 specimens/gram sediment (post-compacted) and remains at abundances around 450,000 specimens/gram sediment up to about the 71 m level. Continued up to 68.5 m the abundance varies between 320,000 and 360,000 specimens/gram sediment, and from 68 to 66 m the abundance drops to between 107,000 and 152,000 specimens/gram sediment. From 65.5 m and up to the uppermost studied sample at 58.2 m the abundance drops further and is reduced to between 50,000 specimens/gram sediment (at 64.5 m) to around 500 specimens/gram sediment (at 59.0 m). This prolific acme is interpreted to reflect a dramatic change in environmental conditions in relation with the impact and just

thereafter. Smelror et al. (2002) suggested that the algal bloom was induced by the enormous amounts of nutrients released into the water column by the impact and the following tsunami. The brief, dramatic change in the depositional conditions and new environmental setting created a unique opportunity for opportunistic and disaster species such as the *Leiospheridia*.

In the post-impact "algal bloom" interval only a monospecific assemblage, with few foraminifera (i.e., *Trochammina* aff. *Septentrionalis*) is found (Bremer et al. 2004) (Fig. 5.15). Above 67 m the diversity and abundance of foraminifera increase somewhat, but in spite of this faunal expansion the diversity is still low. The assemblages are dominated by agglutinated taxa but there are also a few calcareous forms present in the samples at 66.0 and 60.0 m. The faunas are dominated by *Evolutionella vallata*, *Gaudryina rostellata*, *Recurvoides obskiensis* and *Trochammina* spp. (Bremer et al. 2004) (Fig. 5.15). These assemblages closely resemble those found in the Agardhfjellet Formation on Svalbard. These observations of the benthic foraminifera faunas suggest that "normal" (pre-impact) oceanographic and depositional conditions of the Hekkingen Formation environments were restored at the time of deposition of the sediments above 67 m in the Mjølnir core 7329/03-U-01.

The duration of the aftermath, covering the time of the prasinophycean bloom and ocean eutrophication is hard to determined precisely, but most likely took place during a relatively short time. This means we have to assume a very high sedimentation rate to account for the about 7–8 m of post-impact dark shales containing the *Leiosphaeridia* bloom and the monospecific foraminifera assemblage. This depositional rate is extreme for such fine-grained sediments, but not unlikely given the fact that about 233 km^2 of sea-bottom sediments and underlying bedrock were thrown up and spread in the water columns and air in a few seconds (Shuvalov et al. 2002). From the subsequent fall-back and resurge much of the sediments were brought back in the crater, including some organic-rich sediments from the target area and more distal areas agitated by the tsunamis.

Only a sparse macrofauna has been recovered from the Mjølnir crater core and adjacent boreholes. This is because the cores are only 5 cm in diameter, and because the anoxic to hypoxic depositional environments of the Hekkingen Formation contained relatively sparse benthic communities. Based on the available material no dramatic changes have been registered in our collections. This is, however, to be expected for an impact of this size (Smelror et al. 2001a; Bremer et al. 2004).